Computational High-Pressure Chemistry: Ab Initio Simulations of Atoms, Molecules and Extended Materials in the Gigapascal Regime

Authors:
Felix Zeller[1] (Email: zellerf@uni-bremen.de; ORCID: 0000-0001-9140-8359)
Chieh-Min Hsieh[1] (Email: chsieh@uni-bremen.de; ORCID: 0000-0002-9206-4524)
Wilke Dononelli[2,3,4] (Email:wido@uni-bremen.de; ORCID: 0000-0001-7577-421X)
Tim Neudecker*[,1,2,3] (Email: neudecker@uni-bremen.de; ORCID: 0000-0001-7599-3578)

[1] University of Bremen, Institute for Physical and Theoretical Chemistry, Leobener Straße 6, D-28359 Bremen, Germany
[2] Bremen Center for Computational Materials Science, Am Fallturm 1, D-28359 Bremen, Germany
[3] MAPEX Center for Materials and Processes, Bibliothekstraße 1, D-28359 Bremen, Germany
[4] University of Bremen, Hybrid Materials Interfaces Group, Am Fallturm 1, D-28359 Bremen, Germany

* Corresponding author

Abstract:

The field of liquid-phase and solid-state high-pressure chemistry has exploded since the advent of the diamond anvil cell, an experimental technique that allows the application of pressures up to several hundred gigapascal. To complement high-pressure experiments, a large number of computational tools have been developed. These techniques enable the simulation of chemical systems, their sizes ranging from single atoms to infinitely large crystals, under high pressure and the calculation of the resulting structural, electronic and spectroscopic changes. At the most fundamental level, computational methods using carefully tailored wall potentials allow the analytical calculation of energies and electronic properties of compressed atoms. Molecules and molecular clusters can be compressed either via mechanochemical approaches or via more sophisticated computational protocols using implicit or explicit solvation approaches, typically in combination with Density Functional Theory, thus allowing the simulation of pressure-induced chemical reactions. Crystals and other periodic systems can be routinely simulated under pressure as well, both in a static and in a dynamic manner, to predict the changes of crystallographic data under pressure and high-pressure crystal structure transitions. In this review, the theoretical foundations of the available computational tools for simulating high-pressure chemistry are introduced and example applications demonstrating the strengths and weaknesses of each approach are discussed.

Contents

1 Introduction

Using modern high-pressure technology,[1–7] a plethora of fascinating effects can be induced in chemical systems. Pressure in the gigapascal range (1 GPa $\approx 10^5$ atm) may cause electronic rearrangements at the atomic level,[8,9] allows the synthesis of otherwise unobtainable chemical compounds,[10] gives access to novel crystal structures,[11] and leads to the metallization[12] or polymerization of substances.[13] The experimental method of choice in high-pressure chemistry, physics and materials science is the diamond anvil cell (DAC),[1,14] which allows the constant application of pressure up to a few hundred GPa.[15] Due to this enormous pressure range, even planetary interiors can be modeled with a DAC.

The intriguing electronic, structural and spectroscopic effects observed in high-pressure experiments cannot be fully understood and appreciated, if experiments are carried out on a standalone basis. To complement high-pressure experiments, a cornucopia of computational tools have been developed. Some of these approaches have been the focus of previous review articles, e.g., simulation methods for molecules,[16,17] crystals[11,18–23] and biological systems[24] under pressure. This review article presents and overview of *ab initio* computational methodologies spanning the entire range between the atomic scale and infinitely large periodic systems under pressure. The theoretical foundations of each of these computational tools are summarized (Section 2) and selected applications, demonstrating the capabilities − and limitations − of modern computational high-pressure chemistry, are pointed out (Section 3).

It is important to differentiate between pressure that is applied to a substance externally, e.g., using a DAC, and internal/chemical pressure that arises from lattice strain.[25,26] Similarly, the application of hydrostatic/isotropic pressure often yields different results than non-hydrostatic/anisotropic compression.[27,28] Here, the focus lies on externally applied hydrostatic pressure.

2 Simulation Techniques

2.1 Some Introductory Remarks

2.1.1 A Brief Historical Overview

Because pressure is a classic thermodynamic state variable, it has appeared in equations since the beginning of thermodynamics.[29] Later, in the first half of the 20th century, seminal contributions have appreciated the role of pressure in quantum mechanics[30] and its influence on chemical reactivity.[31] Turning to high-pressure *ab initio* simulations, early work presented Self-Consistent Field (SCF) calculations of quantum mechanical systems under pressure,[32,33] e.g., a hydrogen atom in a box.[34] Placing atoms and small molecules in boxes confined by wall potentials is a fruitful endeavor and such approaches are still being developed today (Section 2.2).

The field of computational high-pressure chemistry was boosted tremendously by the development of barostats in the 1980s.[35–38] Barostats play a central role for high-pressure simulations, since they are a crucial ingredient for Molecular Dynamics (MD) simulations − sometimes in combination with Density Functional Theory (DFT) −, thereby paving the way for studying the time propagation of extended systems under pressure.

Moreover, in the 1980s a general expression for the macroscopic stress tensor was presented, which enables static DFT calculations of bulk systems under pressure.[39] However, from a quantum mechanical point of view, it must be noted that none of the terms in the electronic Hamiltonian includes pressure as an explicit variable. This complicates the calculation of electronic energies and molecular properties using DFT and wavefunction-based simulation methods. Only within the past 15 years or so, specialized approaches have been developed that circumvent this problem and allow the simulation of pressure at the molecular level (Section 2.3). These approaches facilitate the comparison of high-pressure single

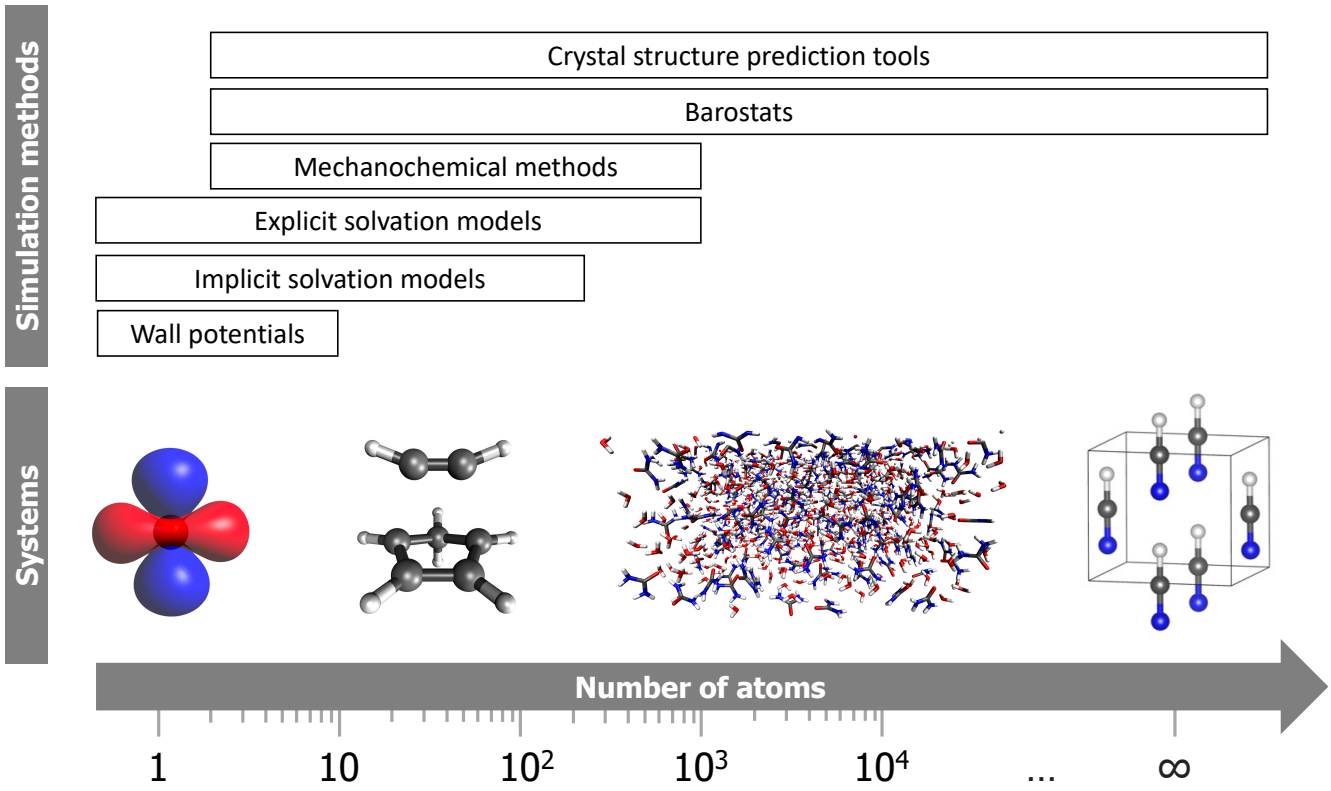

Figure 1: Schematic representation of system sizes typically covered by different high-pressure simulation tools.

molecule and bulk effects. Moreover, the full power of *ab initio* simulation methods for, e.g., bonding and interaction analyses, as well as calculations of a wealth of pressure-induced spectroscopic effects can be exploited.

Today we have the luxury of choosing between a variety of simulation tools for systems of all sizes under pressure, ranging from single atoms to infinitely large materials (Figure 1). The connection between the different length scales is established in Section 2.1.2.

2.1.2 Bridging Length Scales and Relating Model Concepts to the Real World

Often, text books of quantum mechanics start with the example of the hydrogen atom. This system only consists of a proton and an electron, and an exact solution of the Schrödinger equation is possible. Hydrogen is also the focus of many high-pressure studies using wall potentials (Section 2.2), and often

analytical solutions for energies and other observables are available. As soon as the system size increases, however, approximations have to be used. In quantum chemistry, wave function based methods are often applied, ranging from the mean-field Hartree-Fock (HF)[40,41] theory to more systematically accurate *ab initio* correlation methods like MP2[42] or CCSD(T).[43–45] The latter method is often referred to as the "gold standard of quantum chemistry". Unfortunately, these high-level methods, especially CCSD(T), can only be used for small molecules with less than 50 atoms. We note, however, that there is ongoing research to accelerate the speed of these calculations to be able to simulate systems containing several hundreds of atoms by introducing additional approximations.[46–50]

Nevertheless, for most quantum chemical calculations, DFT is used to describe the electronic structure of the system of interest, since system sizes up to a few hundred to a thousand or so atoms can be modeled. Depending on the choice of the exchange correlation (XC) functional, observables of different classes of materials can be calculated with good agreement to experimental observations. As shown in Section 3, DFT is used for most studies in computational high-pressure research, too. In these studies, molecules are simulated either in an isolated way (Section 2.3.1) or, alternatively, in confined environments like in (implicit) solution (Section 2.3.2). If more than one molecule shall be considered or the interaction with the environment needs to be taken into account, explicit solvation models can be applied (Section 2.3.3). However, for treating long-range interactions accurately, calculations are usually performed using periodic boundary conditions (Section 2.4). This methodology allows for simulations of well ordered crystalline structures and phase transitions, e.g., between the liquid and the solid phase.

Even if a high-level method like CCSD(T) or a very accurate XC functional is used in atomistic simulations, still a comparison to real world experimental observations might not be straightforward. One reason is that, most commonly, gas phase molecules are represented by modelling only a single static instance of the molecule. However, this assumption might only be correct at 0 K, since, at higher temperatures, vibrations and rotations will change the structure. To address this problem, statistical effects

have been appreciated in high-pressure experimental/computational studies early on.[51] Another aspect, which has recently been discussed, e.g., in the field of conceptual density function theory, is the inclusion of external electronic or magnetic fields to the simulations to mimic experimental conditions.[52,53]

The main reason why it is often difficult to compare the outcomes of experiments and calculations is the computational resources that are available nowadays. Therefore, the need of experimental model studies that can be compared to theoretical calculations is crucial. In the context of heterogeneous catalysis, Sauer and Freund discussed the benefit of such model studies to identify factors that determine the properties of catalytic materials with respect to reactions by systematically increasing the complexity of the system.[54] Similar approaches are needed and used in the context of high pressure research. One example is a study of McWilliams et al., who investigated processes in planetary interiors in an experimental model study of phase transitions of MgO, which is abundant on terrestrial planets.[55] The same system has then been investigated by Holmström and Stixrude with first-principles free-energy calculations to predict a pressure-induced spin crossover in the liquid planetary material (Mg,Fe)O.[56] Synergistic efforts like these enable refinements of the simulation techniques and make a crucial contribution towards increasing their reliability.

2.2 Atoms and Small Molecules in Confining Potentials

The idea of describing the compression of an atom by placing it in a box with impenetrable walls dates back to the very early days of quantum chemistry and was first studied by Michels et. al in 1937 in an approximate manner.[30] Soon after, the problem was solved formally for the confined hydrogen atom by Sommerfeld and Welker.[57] Since then, this approach has continuously been extended to study atoms and small molecules under compression, as well as to model atoms in molecular cages such as fullerenes or zeolites.[58] Considering the amount of research conducted throughout the past 85 years, a comprehensive

and in-depth analysis of all methods would certainly exceed the limits of this review. We here aim to give a non-exhaustive overview over the basic ideas and highlight the series "Theory of Confined Quantum Systems" in *Advances in Quantum Chemistry* for an excellent collection of detailed reviews on the field.[59,60]

The hard-walled box, as introduced by Michels,[30] takes the form of an impenetrable sphere with radius r_C around the center of mass and may be described by adding the external potential $V_{\text{ext}}(r)$ to the Hamiltonian

$$V_{\text{ext}}(r) = \begin{cases} 0, & r < r_C \\ \infty, & r > r_C \end{cases} \tag{1}$$

where r describes the distance to the center of mass. This changes the Dirichlet boundary condition, which requires the wave function to vanish at infinity ($\Psi(\infty) = 0$), to the wave function vanishing at the location of the wall ($\Psi(r_C) = 0$). The corresponding wave function of the hydrogen atom[57,61–66] and mono- and diatomic one-electron systems[67,68] can be solved exactly, making them interesting model systems.

Alternatively, Rayleigh-Schrödinger perturbation theory[69–72] or variational approaches can be used by adding a cutoff term to the basis functions, which forces the wave function to vanish at r_C,[34,73] thus allowing the treatment of many-electron systems.[70,74–78] To study diatomic molecules, the box shape is usually changed to that of a spheroid (ellipsoid), as introduced by Cottrell.[78]

The model of a hard sphere confining a quantum system does not allow for any other interaction with the surrounding than Pauli repulsion and thus can only be seen as a crude approximation of reality. As Connerade pointed out, the infinite potential wall makes the system unobservable and thus violates a basic principle of quantum mechanics.[58] Consequently, it is not surprising that the hard-sphere confinement method cannot accurately reproduce experimental results, as for example the vibrational frequency shifts

of the hydrogen molecule.[76] As a remedy, Ley-Koo et al. proposed the use of a finite constant potential U_0 to study the hydrogen atom,[79] such that

$$V_{\text{ext}}(r) = \begin{cases} 0, & r < r_C \\ U_0 + \frac{1}{r}, & r > r_C \end{cases} , \tag{2}$$

where the $\frac{1}{r}$ term cancels the Coulomb term. The $\frac{1}{r}$ term may also be disregarded, yielding a slightly differently shaped potential.[80] The finite potential approach leads to a significantly better agreement with experimental results for the hydrogen atom, and the same was later found by Gorecki et al. in a study of the confined molecular hydrogen ion.[71] Besides using a step potential, also linear,[71] harmonic[69,81,82] and power series potentials[80,83] have been used. If a power series potential of the form

$$U_0 = \left(\frac{r}{r_0}\right)^N \tag{3}$$

is used, the "stiffness" of the wall can be modeled by the parameter N, where the system rapidly converges to the hard-wall limit for $N \to \infty$.[80,83]

Besides providing a more realistic picture, finite confining potentials provide a grand technical advantage: They do not change the Dirichlet boundary condition and thus can be used with unmodified Gaussian basis sets, allowing an easy implementation in modern quantum chemistry packages.[83]

The pressure P acting on a closed quantum system, i.e., one with impenetrable walls, can be calculated from the virial theorem for the confined system as[84]

$$P(r_C) = -\frac{\partial E}{\partial V_C} = -\frac{1}{4\pi r_C^2}\frac{\partial E}{\partial r_C} , \tag{4}$$

where V_C is the box volume. It has been shown that eq. 4 also holds for an open quantum system, i.e., finite potential walls.[80,85]

A severe limiting factor for confinement potential models is the shape of the box. Hence, mostly atoms, linear or very small molecules such as ammonia[75] or methane[83] have been studied. Approaches to study larger molecules are discussed in the following section.

2.3 Isolated Molecules and Molecular Clusters

2.3.1 Mechanochemical Methods: G-FMPES and (X-)HCFF

Mechanochemistry is the branch of chemistry in which mechanical forces are used to initiate chemical transformations.[86–88] These forces can of course be compressive, and indeed the connection between mechano- and high-pressure chemistry has been pointed out.[89] However, while *ab initio* simulation methods have been developed that apply stretching forces on molecules by constraining coordinates during geometry optimizations[90] or by adding stretching potentials to the electronic energy,[91–93] only in recent years the quantum mechanochemistry community started to investigate compression forces in more detail.

The earliest attempt to model pressure within a mechanochemical framework was the *Generalized Force-Modified Potential Energy Surface* (G-FMPES)[94] model, where an external potential $V_{\text{ext}}(\boldsymbol{R})$ is added to the unperturbed Born-Oppenheimer potential energy surface (PES) $V(\boldsymbol{R})$

$$\overline{V}(\boldsymbol{R}) = V(\boldsymbol{R}) + V_{\text{ext}}(\boldsymbol{R}), \tag{5}$$

yielding the *force-modified* PES $\overline{V}(\boldsymbol{R})$. In the G-FMPES model, $V_{\text{ext}}(\boldsymbol{R})$ is described as the path integral between a geometry $\boldsymbol{R}$ and a relaxed reference geometry $\boldsymbol{R}_{\text{ref}}$ in a conservative force field $\boldsymbol{F}_{\text{ext}}(\boldsymbol{s})$

$$V_{\text{ext}}(\boldsymbol{R}) = \int_{\boldsymbol{R}}^{\boldsymbol{R}_{\text{ref}}} \boldsymbol{F}_{\text{ext}}(\boldsymbol{s})\, d\boldsymbol{s}. \tag{6}$$

Pressure can be simulated by defining compressive forces $\boldsymbol{f}_{\text{ext}}^{(j)}$ acting on the nuclei j as

$$\boldsymbol{f}_{\text{ext}}^{(j)} = K(\boldsymbol{r}_j - \boldsymbol{c}), \tag{7}$$

where $\boldsymbol{c}$ is the center of mass of the system and K a user-defined variable with units $kcal/\mathring{A}^2$, which scales the pressure. The resulting force field corresponds to putting the nuclei into a parabolic potential centered at $\boldsymbol{c}$. The compression force field $\boldsymbol{F}_{\text{ext}}$ is added to the nuclear gradient during a geometry optimization, converging at a stationary point on the pressure-modified PES.

The pressure acting on the system is approximated as the average force acting on an averaged surface of spheres denoted by the distance of the respective atom to $\boldsymbol{c}$ (Figure 2) *via*[95]

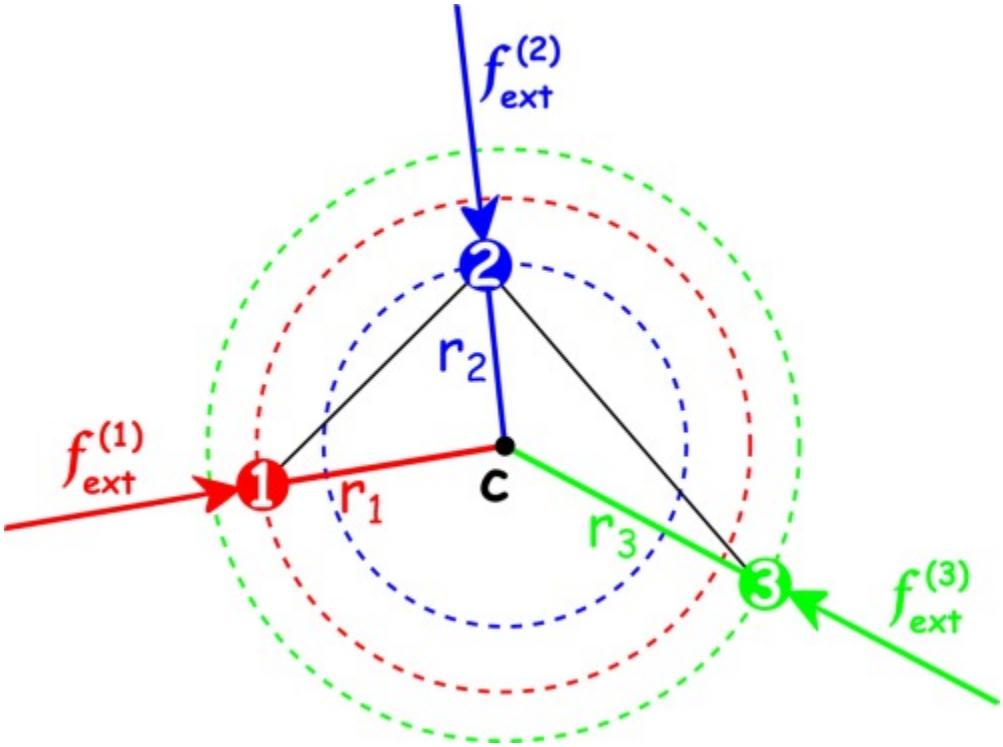

Figure 2: Visualization of external forces and the respective spheres used within the G-FMPES model. Reprinted with permission from Todde et al.,[96] Copyright 2017, Wiley Periodicals, Inc.

$$P_{\text{macro}} = \frac{\langle ||\boldsymbol{f}_{ext}|| \rangle}{\langle A \rangle}. \tag{8}$$

The Hydrostatic Compression Force Field (HCFF)[97] modifies the G-FMPES approach by introducing an upper boundary f_{max} to the individual forces, using the classical definition of pressure, as

$$f_{\text{max}} = P_{\text{guess}} \cdot A_{\text{VdW}}, \tag{9}$$

where P_{guess} is a user-defined variable in MPa, a physically intuitive unit, and A_{VdW} is the Van-der-Waals surface of the investigated molecule, calculated using a Lebedev grid discretization algorithm.[98] The compression force field then takes the form

$$\boldsymbol{f}_{\text{ext}}^{(j)} = f_{\text{max}} \frac{(\boldsymbol{c} - \boldsymbol{r}_j)}{r_{\text{max}}}, \tag{10}$$

where r_{max} is the distance between the center of mass $\boldsymbol{c}$ and the outermost atom. The macroscopic pressure can again be calculated using eq. 8, where $\langle A \rangle$ is replaced with A_{VdW}. Accordingly, the user-defined pressure P_{guess} acts as an upper boundary to P_{macro}.

Both G-FMPES and HCFF suffer from two drawbacks: Firstly, the user can only guess the simulated pressure when setting up a calculation. Secondly, atoms are always pushed to the center of mass of the molecule, leading to unphysical, sphere-like geometries for extended systems, such as alkanes, if high pressure is applied. The eXtended Hydrostatic Compression Force Field (X-HCFF)[99] approach solves these drawbacks by defining forces $\boldsymbol{f}_{ij}$ acting perpendicular to the discretized Van-der-Waals surface of a molecule from each discretization point i to the closest atom j. The force is scaled using the classical definition of pressure as

$$\boldsymbol{f}_i^{(j)} = P \cdot A_i \cdot \boldsymbol{n}_i, \tag{11}$$

where P is the user-defined pressure, A_i the discretized area of the surface point i and $\boldsymbol{n}_i$ the normal vector at i. The respective force acting on atom j is then obtained as the sum of all forces acting on j as

$$\boldsymbol{f}_{\text{ext}}^{(j)} = \sum_{i=0}^{N_{\text{tess}}(j)} \boldsymbol{f}_i^{(j)}, \tag{12}$$

where each discretized surface area that belongs to atom j makes a contribution to the (strictly hydrostatic) compressive force. The resulting force field is added during a geometry optimization, until the restoring force of the molecule cancels the compression force field. It should be noted that the form of the potential causing $\boldsymbol{F}_{\text{ext}}^{\text{X-HCFF}}$ is not parabolic, making the evaluation of eq. 6 nontrivial. Both HCFF and X-HCFF are implemented in the Q-Chem program package.[100]

2.3.2 Implicit Solvation Models: XP-PCM and GOSTSHYP

The Polarizable Continuum Model (PCM) is a well established framework to describe various kinds of solvation interactions implicitly within a quantum chemical calculation.[101–103] The foundation of PCM is the extension of the molecular vacuum Hamiltonian $\hat{H}_0$ with a new term $\hat{V}_{\text{el}}$, describing the Coulomb interaction of the electrons of the solute and a solvent charge density located outside the solute cavity C, thus allowing the calculation of the free energy of the solute, G_{el}, as

$$G_{\text{el}} = \langle \Psi | \, \hat{H}_0 + \frac{1}{2} \hat{V}_{\text{el}} \, | \Psi \rangle \, . \tag{13}$$

In 2008, Cammi *et al.* proposed to model pressure effects by adding a Pauli repulsion term $\hat{V}_{\text{rep}}$ to the PCM Hamiltonian,[104] penalizing the electron density of the solute lying outside its cavity, in the form

$$G_{\text{el-rep}} = G_{\text{el}} + G_{\text{rep}} = \langle \Psi | \, \hat{H}_0 + \frac{1}{2}\hat{V}_{\text{el}} + \hat{V}_{\text{rep}} \, | \Psi \rangle \, . \tag{14}$$

G_{rep} can be calculated as

$$G_{\text{rep}} = \frac{4\pi}{0.7} \, \rho_S \, n_{\text{val}} \int_{\boldsymbol{r} \notin C} \hat{\rho}_M(\boldsymbol{r}) \, d\boldsymbol{r}, \tag{15}$$

where ρ_S is the solvent density, n_{val} its number of valence electrons and the integral denotes the charge density of the solute, located outside its cavity, with $\hat{\rho}_M(\boldsymbol{r})$ being the electron density operator. The pressure P can then be calculated by shrinking the solute's cavity volume V_C using

$$P = -\left(\frac{\partial G_{\text{el-rep}}}{\partial V_C} \right). \tag{16}$$

In practice, V_C is approximated as the volume of fused spheres with the Van-der-Waals radii of the respective atoms and varied by scaling the Van-der-Waals radii. The procedure is illustrated in Fig. 3 and forms the basis of the eXtreme Pressure Polarizable Continuum Model (XP-PCM) framework,[105] which has continuously been evolved over the past fifteen years.[106–114]

Recently, the pressure-modified PES $G_t(P, \boldsymbol{R})$ has been calculated as the Legendre transform of $G_{\text{el-rep}}$,[113]

$$G_t(P, \boldsymbol{R}) = G_{\text{el-rep}}(\boldsymbol{R}) + P V_C(\boldsymbol{R}), \tag{17}$$

where P is calculated analytically by evaluating eq. 16[110] and V_C is the volume of the cavity used to evaluate $G_{\text{el-rep}}$. This implementation allows for a dynamically changing cavity during geometry optimization steps.

In the Gaussians On Surface Tesserae Simulate HYdrostatic Pressure (GOSTSHYP) model,[115,116]

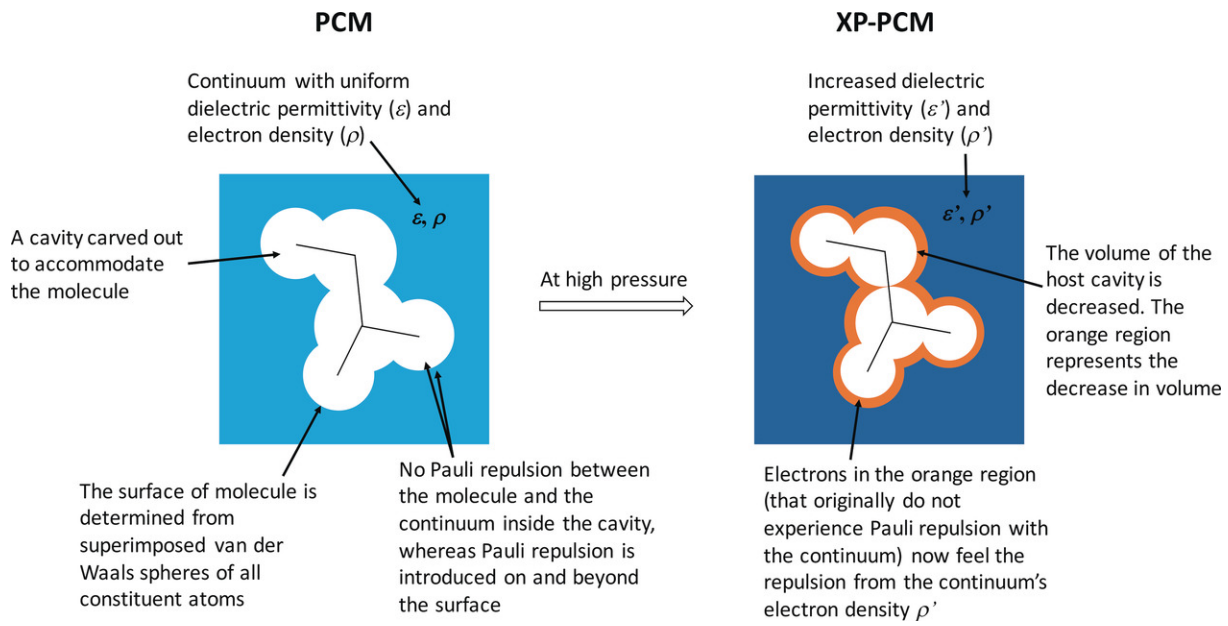

Figure 3: Schematic representation of the XP-PCM approach. Reprinted with permission from Cammi et al.,[108] Copyright 2017, Wiley-VCH Verlag GmbH & Co. KGaA.

similar to XP-PCM, a distortion potential term $\hat{V}_p$ is added to the Hamiltonian, leading to the free energy G_p,

$$G_p = \langle \Psi | \, \hat{H}_0 + \hat{V}_p \, | \Psi \rangle \, . \tag{18}$$

$\hat{V}_p$ describes the interaction with a surrounding arbitrary medium as a sum of Gaussian potentials $\tilde{G}_j$ with the amplitude p_j, centered at each tessera j, that are used to discretize the cavity surface A_C,

$$\hat{V}_p = \sum_{j}^{N_{\text{tess}}} p_j \tilde{G}_j. \tag{19}$$

In contrast to XP-PCM, the cavity is built using pressure-independent Van-der-Waals radii. Pressure is applied by assuming a force equilibrium, where the force resulting from the potential at point j equals the mechanical force $F = P \cdot A_j$ applied to a hard sphere at the point j, leading to the amplitudes p_j as

$$p_j = \frac{P \cdot A_j}{\tilde{F}_j}, \tag{20}$$

where P is the pressure, A_j the area of the tessera j and $\tilde{F}_j$ resembles the response force of the electron gas. The GOSTSHYP model is implemented in the Q-Chem program package.[100] Due to the availability of an energy term and nuclear gradients, geometry optimizations and *ab initio* Molecular Dynamics (AIMD) simulations can be carried out with GOSTSHYP at a user-defined pressure.

Both XP-PCM and GOSTSHYP can be understood as the extension of the finite wall potential approach (Section 2.2) to an arbitrary solvent cavity. It should be highlighted that, in contrast to the previously discussed quantum mechanochemical pressure models, XP-PCM and GOSTSHYP model the influence of pressure on the molecular wave function, allowing a quantum mechanical description of electronic effects, such as dipole moments[115] and electronic excitations,[106] under pressure.

2.3.3 Explicit Solvation Models

In Sections 2.2−2.3.2, methods have been introduced that model the interactions with the surrounding medium in an approximate manner. This allows for a very precise description of the electronic structure of the investigated systems, however, as pressure is a macroscopic quantity, it may be necessary to model the medium more explicitly. In a few model studies, noble gases have been used to function as soft confinement potentials compressing linear systems.[85,117] Miao el al. generalized this approach in the "helium compression chamber" method.[118] Here, an atom is placed in the center of a large periodic box filled with helium atoms modeling the surrounding medium, which is then compressed by reducing the box volume, as shown in Fig. 4. The helium compression chamber has been used to study electrides[118] and, recently, electronegativities.[119]

It must not be forgotten that the approach of using helium atoms as the pressure-transmitting medium is an approximation. In the high pressure regime, this approximation, which models isotropic solvent interaction, does not hold if the "real" solvent has low symmetry. For example, a functional group of the solvent might be pushed into the solute, leading to a stronger local deformation. Hence, it may be

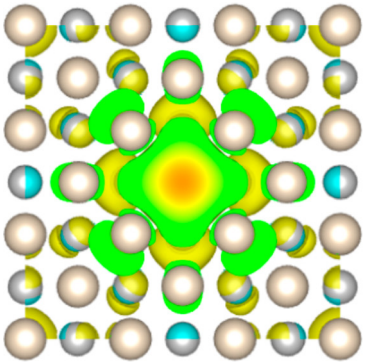

Figure 4: Depiction of helium atoms compressing an inner atom, as used in the helium compression chamber method. Reprinted with permission of Miao et al.,[118] Copyright 2014 American Chemical Society.

necessary to model the structure of the solvent explicitly, which leads to enormous system sizes and, consequently, a high computational cost. Most commonly, such systems are simulated using *ab initio* Molecular Dynamics (AIMD) simulations, which is discussed in Section 2.4.2.

An alternative approach is to model a part of the system using quantum mechanics (QM) and the interaction with the solvent with a molecular mechanics (MM) force field in a combined QM/MM approach. Wiebe, Spooner and co-workers[120,121] proposed a method to calculate the volume V of a compound $\boldsymbol{X}$ in a system of n solvent molecules $\boldsymbol{S}$ as

$$V(\boldsymbol{X}) = V(\boldsymbol{X} + n\boldsymbol{S}) - V(n\boldsymbol{S}), \tag{21}$$

where $V(\boldsymbol{X} + \boldsymbol{n}\boldsymbol{S})$ is the volume of the the solvent droplet containing $\boldsymbol{X}$ and $V(n\boldsymbol{S})$ is the volume of the unperturbed system. Both volumes are obtained as the average volume in an isothermal MD run. The activation volume $\Delta V^{\dagger}$, a crucial observable in high-pressure chemistry (cf. also Section 3.2), can then be calculated as

$$\Delta V^{\dagger} = V\boldsymbol{X} - V(\boldsymbol{X}'), \tag{22}$$

where $\boldsymbol{X}'$ is the transition state. $V(\boldsymbol{X}')$ is calculated by constraining the reaction coordinate, identified by a classical QM calculation, within the MD run. The model was later extended to approximately calculate the pressure-modified potential energy surface (PMPES) $G(\boldsymbol{x}, P)$ as[122]

$$G(\boldsymbol{x}, P) = U_0(\boldsymbol{x}) + PV(\boldsymbol{x}, P), \tag{23}$$

where $\boldsymbol{x}$ is a vector of reaction coordinates, $U_0(\boldsymbol{x})$ the gas phase energy obtained quantum mechanically and $V(\boldsymbol{x}, P)$ is obtained *via* eq. 21 by neglecting its pressure dependence.[122]

While this approach leads to activation volumes in good agreement with experimental data and model systems, it cannot describe the response of the electronic wave function to the compression, limiting the applicability to spectroscopic properties. This can be achieved by embedded-cluster (EC) methods, such as the embedded cluster reference interaction site model (EC-RISM).[123] In the EC-RISM methodology, the solvent is approximated by point charges surrounding the solute and adding the interaction term to the Hamiltonian of the solute. This changes the wave function of the solute and, accordingly, the polarization of the solvent, which again changes the point charges. This procedure is continued until the wave function of the solute converges. To calculate the point charges, the pure solvent susceptibility χ is needed, which is extracted from a previous MD or integral equation based RISM calculation. Thus, the pressure can be modeled indirectly by adjusting the box volume of the underlying MD/RISM calculation.[124] EC-RISM calculations have successfully been used to calculate pressure-dependent Raman[125] and NMR[126] shifts. The model was recently adapted to predict pressure-dependent free solvation energies.[127] Further applications are pointed out in Section 3.2.

Molecular crystals can also be modeled using the binary interaction method (BIM),[128,129] which follows an embedded fragmentation ansatz.[130] Within BIM the enthalpy H of a unit cell is calculated as[128]

$$H = \sum_i E_{i(0)} + \frac{1}{2} \sum_{\boldsymbol{n}} \sum_{ij}{}' (E_{i(0)j(\boldsymbol{n})} - E_{i(0)} - E_{j(\boldsymbol{n})}) + E_M + PV \tag{24}$$

where the indices i and j run over the molecules of the unit cell denoted in brackets, $\boldsymbol{n}$ is the unit cell vector, E_M describes the long range coulomb interactions, P the pressure, V the unit cell volume and the apostrophe denotes the exclusion of the cases $i = j$ and $\boldsymbol{n} = 0$ from the summation. The monomer energies $E_{i(0)}$ and $E_{j(\boldsymbol{n})}$ and dimer energies $E_{i(0)j(\boldsymbol{n})}$ can in principle be obtained at every level of theory, where the crystal field is accounted for by an embedding scheme in dipoles or point charges, obtained by *ab initio* calculations. The pressure is simulated by optimizing the box lattice parameters for a specific pressure. It should be highlighted that BIM does not strictly rely on periodic boundary conditions and therefore is applicable to non-periodic systems.[131] It has been used to extensively study phase diagrams,[131] e.g., of carbon dioxide[132,133] and ice.[134,135] A more detailed discussion of simulated phase diagrams can be found in Section 3.2.2.

2.4 Periodic Systems

Modelling extended systems is computationally very demanding, especially when accurate methods like DFT are used (cf. Section 2.1.2). These extended systems may be non-ordered, like amorphous or liquid materials, or ordered, like polymers, two-dimensional structures (e.g. graphene) or three-dimensional crystal structures. For the latter class of materials, translational symmetry is used to describe the periodic boundary conditions (PBC) in atomistic simulations. Therefore, a periodically repeated box that represents the smallest repeating unit in three-dimensional space, the unit cell, needs to be defined. This unit cell is defined by three lattice vectors, $\boldsymbol{a}$, $\boldsymbol{b}$ and $\boldsymbol{c}$. By multiplying these lattice vectors with integer constants, the system forms an infinite array of replicated cells. The introduction of the unit cell for calculations with PBC leads to a rapid decrease in computation time. However, this is mainly true for

simulations of well-crystalline and highly symmetric materials. As soon as defects in realistic concentrations (less than 1-10 %) have to be considered, a supercell needs to be used, which leads to a rapid increase in computational time.

The motivation for applying pressure in PBC simulations arises from the fact that high-pressure experiments are usually carried out on a large quantity of molecules, e.g., in the form of liquids or crystals. Molecular crystals show well ordered motifs and can be described by a unit cell or super cell as desribed above. On the other hand, description of liquids or amorphous phases is possible, too. In these cases, the cell vectors need to be chosen large enough. Often these cells are referred to as *simulation cells* instead of *unit cells*. While a wealth of structural data of diverse compounds is available under ambient pressure, obtaining structural data under elevated pressure requires increased experimental effort. In such scenarios, simulations yield valuable information. For example, crystal structure prediction (CSP) plays an important role in discovering novel materials. Zurek and Grochala as well as Wang and Ma reviewed various techniques for CSP under pressure,[22,136] and the interested reader is referred to these reviews for further information on high-pressure CSP.

2.4.1 Static Simulations of Periodic Systems under Pressure

As in many other branches of computational chemistry and materials science, periodic systems under pressure are commonly modeled using DFT. Due to the nature of the periodic wave function derived from Bloch's Theorem[137] in such systems, plane-wave basis sets or, more precisely, the projector augmented wave (PAW) method by Blöchl,[138] is typically applied instead of Gaussian Type Orbitals (GTOs) to model the wave function. However, it needs to be kept in mind that PAW calculations are in most cases computationally more expensive than GTO-based calculations.

If a constant external pressure is applied to a solid material, once an equilibrium is achieved, the stress outside of the material must be balanced by the internal counterstress. The stress theorem devel-

oped by Nielsen and Martin establishes a way to calculate the stress tensor induced by an externally applied pressure to a system in PBC simulations.[39,139,140] It is closely related to the force theorem[141] and the quantum mechanical virial theorem.[142–146] In the stress theorem, the Hamiltonian of the system is considered as

$$H = \sum_i \frac{\mathbf{p}_i^2}{2m_i} + V_{\text{int}} + V_{\text{ext}}, \tag{25}$$

where m_i and $\mathbf{p}_i$ represent the mass and the momentum of the ith particle, respectively. The potential energy is separated into two parts: the internal component, V_{int} and the external component, V_{ext}, the latter of which is attributed to the external influence, i.e., pressure. For a deformed many-body system, the stress $T_{\alpha\beta}$ can be expressed as

$$T_{\alpha\beta} = -\sum_i \langle \Psi | \frac{p_{i\alpha} p_{i\beta}}{m_i} - r_{i\beta} \nabla_{i\alpha}(V_{\text{int}}) | \Psi \rangle, \tag{26}$$

where r is the position of the particle, and the indices α and β run from 1 to 3 in a 3-dimensional system. Each combination of $\alpha\beta$ corresponds to a component in the stress tensor. In a periodic system, the average stress density of the system can be defined as $\sigma_{\alpha\beta} = T_{\alpha\beta}/\Omega$, where Ω represents the volume of the unit cell. Moreover, the authors indicate that the viral theorem in its quantum form is a specific case of the stress theorem, shown as

$$3P\Omega = 2\sum_i \frac{\langle \mathbf{p}_i^2 \rangle}{2m_i} - \sum_i \langle \mathbf{r}_i \cdot \nabla_i V_{\text{int}} \rangle, \tag{27}$$

where P denotes the pressure. It is interesting to note that eq. 27 corresponds to the negative trace of eq. 26.

A rather modern approach presented by Bidault and Chaudhuri utilizes the Quasi-Harmonic Approx-

imation (QHA) with an energy correction (EC) formalism to describe the thermal and pressure-induced properties of molecular crystals.[147] In this method, dispersion-corrected DFT optimization is carried out for molecular crystals at different pressures to obtain $U_0(V)$, which represents energy variations with respect to the volume of a system. Subsequently, phonon calculations are applied to these optimized structures, from which the vibrational free energy, $F_{\text{vib}}(V,T)$ can be obtained. Finally, QHA and EC is applied and the resulting Helmholtz free energy is expressed as

$$F(V,T) = U_0(V) + F_{\text{vib}}(V,T) + \frac{\alpha}{V}, \tag{28}$$

where α/V is the EC term and α is a parameter adjusted to restore the volume optimized at zero pressure. It should be noted that this EC term was first proposed by Otero-de-la-Roza and Luaña.[148]

2.4.2 High-Pressure Molecular Dynamics Simulations

The previous section was mainly concerned with calculations of the "static" high-pressure properties of periodic materials. However, in many cases, a more dynamic picture is required, which is commonly achieved by following a Molecular Dynamics (MD) approach. In MD simulations, pressure can be derived as the virial expression[149]

$$P = \frac{Nk_BT}{V} + \frac{1}{3V}\langle\sum_{i=1}^{N}\mathbf{r}_i \cdot \mathbf{f}_i\rangle, \tag{29}$$

where N is the number of interacting atoms contained in a volume V, k_B is the Boltzmann constant, T is the temperature, $\mathbf{r}_i$ represents the position of atom i, and $\mathbf{f}_i$ is the total force acting on atom i. The term enclosed in the angled bracket on the right of the equation is the internal virial, which arises from forces acting between atoms in a system. However, as pointed out by Louwerse and Baerends,[150] this equation is not applicable in PBC. For systems with pair-additive force fields, pressure can be expressed as

$$P = \frac{Nk_BT}{V} + \frac{1}{6V}\langle\sum_{i=1}^{N}\sum_{j\neq i}^{N}\mathbf{r}_{ij}\cdot\mathbf{f}_{ij}\rangle, \tag{30}$$

which is effective for use with PBC. Yet, it is not valid if a non-pair-additive force field is employed.

Later on, this problem was solved by Thompson et al., who derived three virial forms, which are articulated in terms of force contributions to atoms and are independent of interatomic potentials, functioning within the context of PBC.[151] The key idea is to associate each repeating group of atoms with exactly one of the numerous unit cells. As a consequence, the potential energy of the unit cell can be defined as the sum of all potential energy groups associated with the unit cell, represented by

$$U(\mathbf{r}^N) = \sum_{k\in 0} u_k(\mathbf{r}^{N_k}), \qquad \mathbf{r}^{N_k} = \mathbf{r}_1^k, \mathbf{r}_2^k, ..., \mathbf{r}_{N_k}^k, \tag{31}$$

where $\mathbf{r}$ is the position of atoms and $k \in 0$ denotes all groups of atoms associated with the unit cell.

Pressure control in MD simulations is a crucial aspect, and various algorithms, known as barostats, have been developed over the years. In the 1980s, Andersen first ran MD simulations under constant pressure in systems of bulk liquid.[38] Andersen's method, also referred to as the Andersen barostat, allows the volume of the simulation cell to change isotropically and works by adjusting the volume of the simulation cell: If the volume increases, the pressure decreases, and vice versa. In this method, coordinates of atoms $\mathbf{r}_i$ are expressed in scaled coordinates, as

$$\mathbf{r}_i = \Omega^{1/3}\cdot\mathbf{s}_i, \qquad i = 1, 2, ..., N, \tag{32}$$

where N is the number of atoms, Ω is the volume of a cubic simulation box and $\mathbf{s}_i$ is a fraction between 0 and 1. As a result, the Lagrangian, i.e., a function that describes the dynamic behavior of a system, is expressed in terms of new scaled coordinates, depicting a fluid in a container with variable volume. Here,

the fluid can be compressed or decompressed by a piston with a fictitious mass M. It is important to note that the decay of volume fluctuation is influenced by the mass of the piston.

Unlike the Andersen barostat, the Parrinello-Rahman (PR) barostat allows the volume of the simulation cell to change anisotropically, which is well-suited for studying pressure-induced phase transitions of crystals.[37] In the PR method, the simulation box is composed of three vectors ***a***, ***b*** and ***c***, which are allowed to have different lengths and orientations. Similar to Andersen's approach, the scaling of atomic coordinates can be expressed as

$$\mathbf{r}_i = \mathbf{h} \cdot \mathbf{s}_i, \quad i = 1, 2, ..., N, \tag{33}$$

where **h** is a matrix composed of ***a***, ***b*** and ***c***. To model molecular systems, Nosé and Klein incorporated long-range charge-charge interactions, and improved the previous methods by adding a constraint to prevent unnecessary rotation of the MD cell.[36] This method was later advanced by Hoover,[152] and it is commonly referred to as the Nosé-Hoover barostat. Subsequently, Wentzcovitch expanded the scope of the PR approach by making it invariant with respect to the choice of simulation cell.[153]

Berendsen et al. introduced a distinct category of barostats,[35] where an external bath with constant pressure is coupled to a system by incorporating an additional pressure term into the equations of motion,

$$\left(\frac{dP}{dt}\right)_{\text{bath}} = \frac{P_0 - P}{\tau_P}, \tag{34}$$

defining the pressure bath as the difference between the external pressure P_0 and the internal pressure P at a given coupling time τ_P. Nevertheless, it is worth noting that the coupling method does not sample the *NPT* ensemble.

Besides, a Monte Carlo (MC) scheme can also be implemented in the MD pressure control algorithm, which is also referred to as the MD/MC algorithm.[154,155] In MD/MC simulations, the pressure is not

calculated during the process, but instead, the change of cell volume is decided by random numbers within the MC scheme. In terms of application, for instance, Wiebke et al. employed a parallel-tempering Monte Carlo scheme to study the melting temperature of argon under high pressure.[156]

Last but not least, the virtual rotational diamond anvil cell (VRDAC), a modern technique employing quantum-based molecular dynamics (QMD), simulates the compression of materials sandwiched between two diamond slabs. As demonstrated in the work of Steele et al., the mechanochemistry of glycine under compression and shear is simulated using the VRDAC approach.[157]

3 Applications

In many applications of computational high-pressure chemistry, DFT using PBCs is the method of choice.[158–162] In this Section, however, care is exercised to present applications using other methods as well, e.g., wall potentials, mixed quantum mechanical / molecular mechanics (QM/MM) approaches, Quantum Monte Carlo, and single-molecule methods such as (X-)HCFF, XP-PCM and GOSTSHYP.

3.1 Fundamental Properties of Materials at High Pressure

Pressure changes many fundamental properties of atoms and challenges the way we think about basic chemical concepts. Examples include changes in atomic/molecular properties (Section 3.1.1), such as electronic configurations, atomic radii, electronegativity, ionization potentials and electron affinities, aromaticity and bonding patterns. Moreover, we will discuss pressure-induced spin crossover processes (Section 3.1.2) and changes in spectroscopic properties of compressed chemical systems (Section 3.1.3).

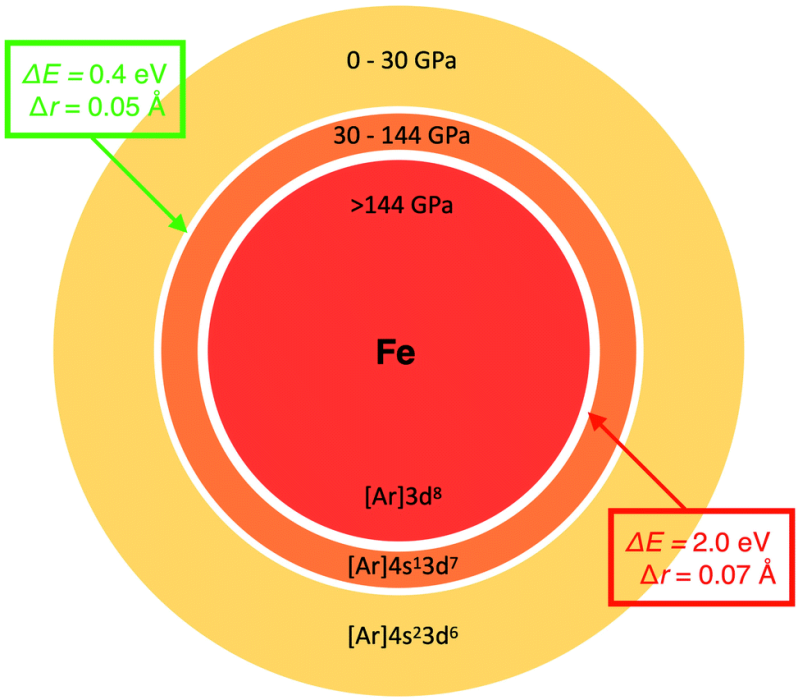

Figure 5: Calculated atomic radius, electronic configuration and energy change in an Fe atom in different pressure regimes. Reproduced with permission from Rahm et al.,[164] Copyright 2021, Royal Society of Chemistry.

3.1.1 Electronic Effects and Chemical Bonding

Efforts to understand chemical structure and reactivity in the GPa regime have motivated investigations of basic high-pressure properties of atoms, the fundamental building blocks of chemical compounds. Non-bonded atomic radii, for example, have been studied with XP-PCM up to 300 GPa.[163] The relative ordering of atomic radii present at ambient conditions was found to be largely retained at higher pressure, with an increase in pressure in most cases leading to a smooth decrease in the atomic radius. A notable exception to this rule is lithium: At 209 GPa, a marked decrease in the atomic radius was observed, which was explained by a change in the electronic configuration from $1s^2 2s^1$ to $1s^2 2p^1$. This demonstrates that electronic configuration and atomic radius are intimately connected, an effect that is demonstrated clearly also in the iron atom (Figure 5).

The change in electronic configurations has been extensively investigated using confinement potentials, and the state-of-the-art was recently was reviewed by Connerade.[58] Most notably it was found

that under high pressures the aufbau principle is followed more strictly by occupying the most compact orbitals first.

A first-order perturbation treatment of XP-PCM allowed more in-depth studies of the compression of atomic orbitals.[8] It was found that diffuse orbitals are being destabilized more significantly by pressure than core orbitals. Clearly, the spatial extension of an atomic orbital dictates how exposed its electrons are. A comprehensive XP-PCM study even presented data on the pressure-dependent electronic configurations of all atoms in the periodic table and allowed to establish a connection to magnetism under pressure.[9] The XP-PCM data on electronic configurations ties in with DFT calculations using PBCs on lithium-beryllium alloys, in which the pressure-induced removal of two electrons from the lithium atoms was observed when the pressure was sufficiently high.[165]

The change in electronegativity with pressure has been studied extensively, since interpreting this quantity allows the rationalization of many chemical reactions. Confining potentials in combination with Hartree-Fock calculations, for example, have been used for investigating electronegativity under pressure.[69] Using XP-PCM, an equation relating atomic radius and electronegativity has been developed.[164] It was found that both decrease with increasing pressure. The same trend was recently found in a study using the helium compression chamber method investigating electronegativiy and chemical hardness under pressure.[119] Additionally, XP-PCM allowed the calculation of electronegativity at shock fronts,[166] and the related calculation of bond polarities and dissociation routes in energetic materials.

Ionization energies and electron affinities have been calculated *via* the second derivative of the energy w.r.t. the scaling factor of the cavity used in XP-PCM.[112] In a combination with Conceptual DFT (CDFT),[167] the derivative of the energy w.r.t. external pressure allowed the calculation of a range of chemical properties and it was found that ionization potentials, electron affinities, electronegativities and polarizabilities decrease upon increasing pressure, whereas the chemical hardness increased.[114]

The above examples demonstrate that pressure influences the electronic structure of atoms funda-

mentally. As a result, the very nature of the chemical bond changes and some astonishing effects can be observed.[168] Noble gases, for example, become reactive under pressure.[169–173] Although it is in many cases unclear whether the interatomic contacts involving noble gas atoms can rightly be called chemical bonds, the observed interactions between noble gases and other species suggest that the concept of the chemical bond must be overthought in the high-pressure regime.

In the extreme case, pressure leads to metallization, i.e., equalization of the electron distribution within a substance.[174] This behaviour was already predicted Sommerfeld and Welker,[57] who, by studying the hydrogen atom in an impenetrable box, found that the electron becomes solely bound by the box rather than the core for small boxes and, consequently, high pressures. Below the metallization threshold, different substances respond to pressure in different ways. DFT calculations using PBCs, for example, have demonstrated that XeF_2 becomes $[XeF]^+F^-$ when the pressure is high enough, i.e., the substance undergoes dissociation into an ionic solid.[175] A curium compound, on the contrary, becomes more covalent under pressure, as evidenced by DFT and multireference calculations.[176] How the character of a bond is influenced by pressure depends on many factors such as the crystal structure, possible interactions between metal atoms and the nature of the metal-ligand bonds.

Reproducing the experimentally observed shortening of chemical bonds under pressure is one of the key tasks of high-pressure simulation techniques. When a novel method is being published, pressure-dependent interatomic distances typically belong to the first quantities to be reported. A relation between pressure and interatomic distances in inorganic crystals has already been established two decades ago using a mathematical model that takes into account the force exerted on the atoms involved in a chemical bond upon compression.[177] The capability of XP-PCM in relating pressure, equilibrium geometries and electron density in chains of hydrogen atoms has been demonstrated as well.[178] GOSTSHYP allows the calculation of the pressure-vs-volume curves of substances, e.g., fullerenes,[116] and, in principle, also the pressure-dependent volume of the electron clouds between atoms involved in a chemical bond.

Turning to molecular properties, a seminal study has demonstrated the loss of aromaticity in an annulene derivative.[179] Experiments in conjunction with PBC and gas-phase DFT calculations have shown that pressure causes a gradual trapping of one of the resonance structures of the compound, which leads to a possible increase in reactivity. In another mixed experimental/computational study, the decrease in aromatic character in a nanohoop structure has been described as well.[180] These studies highlight the connection between high-pressure chemistry and mechanochemistry, where aromatic character can be adjusted using stretching forces.[181]

When discussing the influence of pressure on molecular properties and bond lengths, bond angles etc. within the molecules, it must be kept in mind that intermolecular distances are usually compressed first when applying pressure, due to the higher compressibility of these "soft" degrees of freedom. There is a great diversity of intermolecular interactions, e.g., coulombic and van-der-Waals interactions and hydrogen bonds, and each type of interaction responds to pressure differently.[182] Therefore, depending on the chemical system under consideration, strengthening intermolecular interactions between functional groups by pressure may either be stabilizing[183] or possibly precondition the molecules for polymerization.[184] In the case of hydrogen cyanide (HCN) chains, a mixed PBC, X-HCFF and GOSTSHYP study using DFT showed that the pressure-induced strengthening of the interaction between the nitrogen lone electron pair and the carbon−hydrogen σ^* orbital leads to a lengthening of the carbon−hydrogen bond.[185]

As can be seen from these examples, pressure-induced changes in electronic configurations, atomic radii, chemical bonds and atomic/molecular properties are diverse and, in many cases, system-specific. Studying them is a highly fruitful endeavor, leading to a better understanding of pressure-induced chemistry, while at the same time challenging our understanding of fundamental chemical concepts. Computational methods play a crucial role in these investigations, since they allow in-depth analyses with much more detail than obtainable using experimental techniques only.

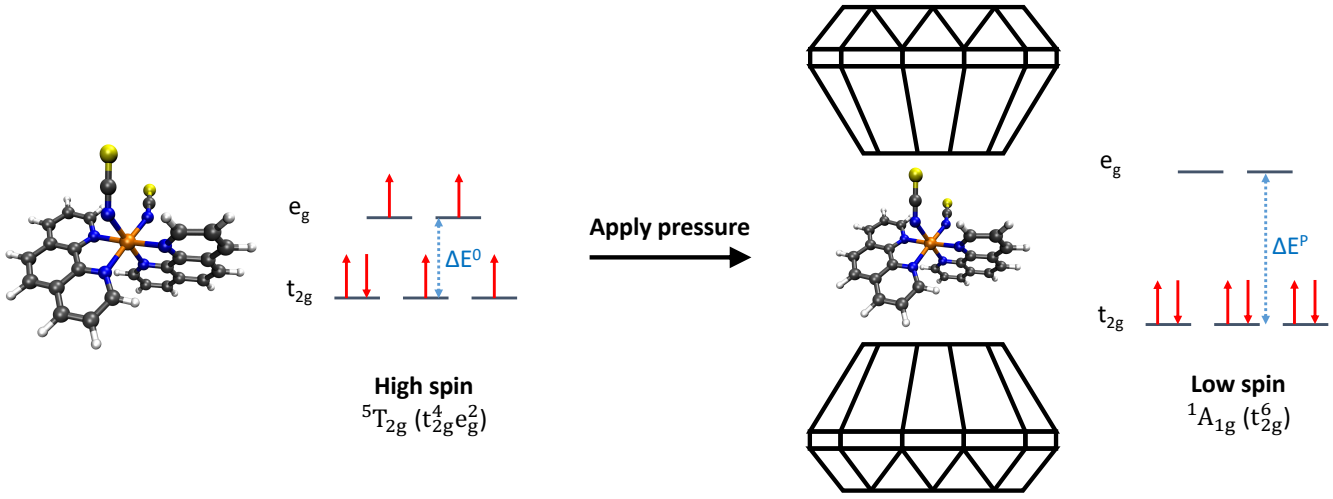

Figure 6: Pressure-induced spin crossover in the archetypal [Fe(phen)$_2$(NCS)$_2$] complex. Pressure leads to a decrease in the metal-ligand distance and to a concomitant increase in the ligand field splitting energy. As a result, a switching from the high spin to the low spin state is observed if the pressure is high enough.

3.1.2 Spin Crossover Processes

In spin crossover (SCO) complexes, two discrete electronic spin states (high spin (HS) and low spin (LS)) are available. The different number of unpaired electrons in the HS and LS states gives access to distinct magnetic and spectroscopic properties. As a result, futuristic applications of SCO complexes in spintronics and as sensing and memory devices have been suggested.[186–188] Transitions between the HS and LS states can be induced by various external stimuli, including pressure.[189–194] An example is the prototypcal [Fe(phen)$_2$(NCS)$_2$] complex, in which pressure leads to a decrease in the metal-ligand distances and to an accompanying increase in the ligand field splitting energy, followed by SCO from the HS to the LS state (Figure 6). Here, the focus lies on pressure-induced SCO in molecular metal-ligand complexes, but it must be noted that polymeric and non-molecular crystalline SCO systems are abundant,[56,195–204] some of which have important implications for the magnetic properties of Earth's interior.

Modern experimental studies on SCO processes, whether they are induced by pressure or not, are usually accompanied by simulations.[205–207] However, conducting such simulations in a meaningful and

reliable way is far from trivial, owing to the intricate interplay between temperature and pressure in the SCO process. The $T_{1/2}$ temperature, i.e., the temperature at which the HS and the LS state are equally populated, is a key observable, which necessitates some statistical analysis. Moreover, it is remarkably difficult to find an accurate wave function based method or density functional that predicts the spin state ordering and the energetic difference between HS and LS states accurately.[208–210] The performance of density functionals in the calculation of the energy difference between HS and LS states has been studied fairly early,[211] and reparameterized density functionals with an optimized amount of Hartree-Fock exchange have emerged as successful tools to reproduce the correct electronic configurations.[212–214]

Despite these technical challenges, a number of computational studies have either successfully reproduced experimental measurements or delivered fundamental insights into the SCO process. The HCFF method, for example, has been used to study octahedral metal-ligand model complexes at the DFT level.[97] It was found that the amount of pressure required to induce SCO in different complexes depends on the position of the ligands in the spectrochemical series. Based on these result, fundamental design guidelines for complexes with a tailored SCO pressure could be deduced.

In a multiscale simulation approach, DFT was used to parameterize iron-nitrogen potentials in the $[Fe(PM\text{-}BiA)_2(NCS)_2]$ (PM-BiA = N-(2-pyridylmethylene)aminobiphenyl) SCO complex, which were subsequently used in MD simulations.[215] This model allowed to probe the delicate interplay between crystalline and single-molecule effects and the influence of these factors on SCO. Finally, a (P,T) diagram for the complex was deduced. Calculating such diagrams is of tremendous help when comparing simulations with experiments, as evidenced by a study presenting an Ising Hamiltonian for a one-dimensional SCO coordination polymer.[216]

Plane-wave DFT using the Hubbard model was applied in a study on the SCO in $[Co(II)dpzca)_2]$, in which a Co^{2+} ion is coordinated by two pyrazine imide ligands.[217] The carefully tailored computational protocol reproduced the experimental pressure-dependent $T_{1/2}$ temperature reliably up to 2500 bar.

Moreover, pressure-dependent crystallographic data and the density of states (DOS) of the compound were simulated accurately.

Several studies have revealed the sensitivity of the SCO behavior to minute structural changes in the immediate surrounding of the central metal ion. DFT and a model Hamiltonian approach, for example, established the connection between the pressure-dependent iron-nitrogen distances and the SCO process in a dinuclear Fe(II) complex.[218] The observation that magnetic properties are very sensitive to small structural changes has been made in a mixed experimental/DFT study on $Co(SPh)_4(PPh_4)_2$, a single-molecule magnet.[219] Moreover, in an investigation using Monte Carlo simulation techniques, the coupling between SCO centers was described as harmonic stretching and bending interactions, highlighting the importance of geometric and vibronic effects in SCO complexes.[220]

These examples demonstrate that, while the computational modeling of (pressure-induced) SCO is a highly challenging endeavor, several examples prove that today's simulation methods can be used to gain both fundamental and practical insights into SCO processes. Further methodological advancements in the underlying electronic structure theory as well as the development of multiscale simulation approaches will surely continue to contribute to our understanding of SCO processes at the molecular level.

3.1.3 Spectroscopic Properties: Piezochromism and Vibrational Spectra

The field of high-pressure molecular spectroscopy has been continually growing since the early days of high-pressure research.[221] This is partly due to the necessity to characterize the compounds under consideration *in situ* to detect pressure-induced structural changes or to monitor the progress of a chemical reaction directly within a DAC. Additionally, the changes in spectroscopic properties of compounds that are induced by pressure can be exploited in fascinating ways.

One example is piezochromism, i.e., the change in optical signals upon pressure application. The term "piezochromism" often refers to changes in color, fluorescence or phosphorescence induced either

by hydrostatic compression using, e.g., a DAC, or *via* grinding. However, it is important to note that isotropic compression and grinding setups are vastly different,[222] which may lead to completely different spectroscopic signals.

Piezochromism in non-molecular solids has been studied extensively, e.g., in perovskites,[223–227] but the focus here lies on molecular compounds. In this realm, it has been noted that different crystal structures may yield different piezochromic responses.[228]

A tremendous amount of effort has been devoted to quantifying the effects of pressure-induced intramolecular structural changes and intermolecular interactions on piezochromism.[229] At the single-molecule level, the compression of a molecular scaffold should intuitively cause a blue shift of the UV/Vis absorption bands, as suggested by the particle-in-a-box model. In fact, XP-PCM in combination with symmetry-adapted cluster configuration interaction (SAC-CI) has shown that some absorption bands in the furan molecule are blue shifted under pressure.[106] However, the authors of this study pointed out that, experimentally, a red shift is observed, which is likely due to intermolecular effects. Nevertheless, the value of computational methods like XP-PCM lies in the fact that they allow in-depth analyses of single-molecule effects in piezochromic materials.

In many experiments, a spectroscopic red shift of absorption and fluorescence signals is observed upon pressure application.[230] DFT using PBCs or QM/MM approaches are often used to identify the intermolecular interactions responsible for this effect, e.g., $\pi-\pi$ and CH$-\pi$ interactions (Figure 7).[231–235] In a mixed experimental/computational study it was found that intermolecular interactions may even become so strong under pressure that an electron can be transferred, which has tremendous influence on the piezochromic behavior of the system.[236]

At the molecular level, minute changes in dihedral angles, e.g., those modulating the overlap of neighboring π systems, or the planarity of individual π systems play an important role in piezochromic behavior.[235,237–240] A QM/MM study by Zhao et al., e.g., compared the conformationally flexible diben-

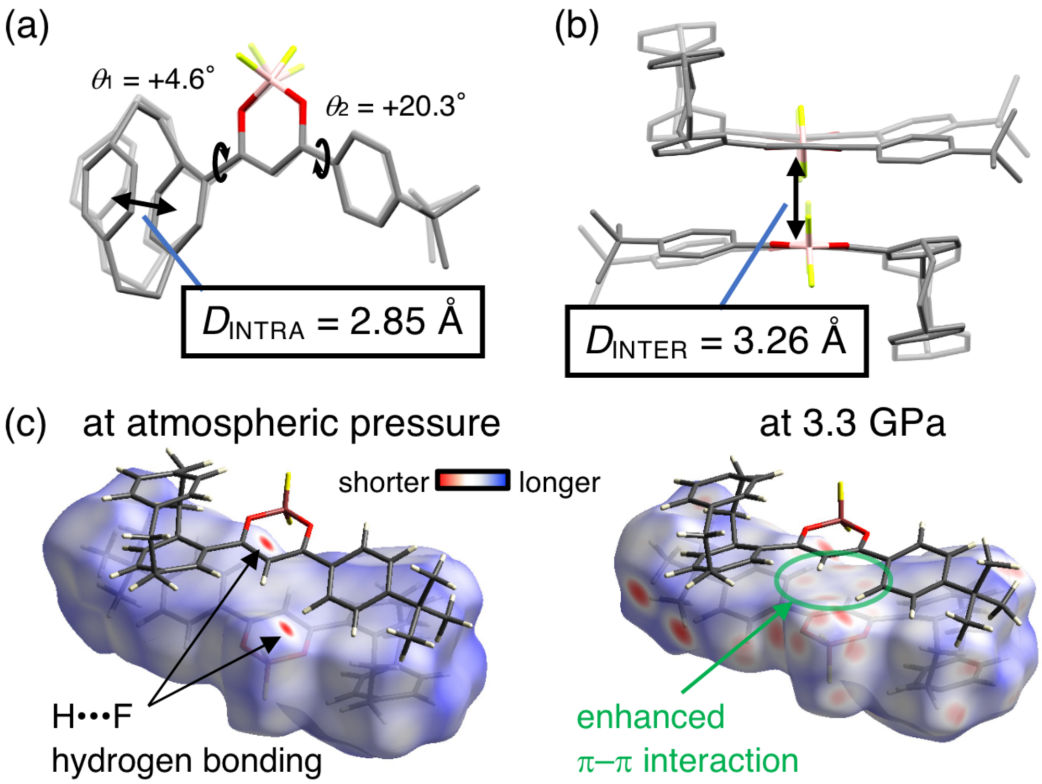

Figure 7: Comparison of intra- and intermolecular effects in a piezochromic paracyclophane-containing organoboron crystal reported by Irii et al.[232] a) Superimposed view of the compound (H atoms omitted) at P = 1 atm (thin) and P = 3.3 GPa (solid). b) Analogous superimposed side view of the π stacking dimer. c) Hirshfeld surfaces at P = 1 atm (left) and P = 3.3 GPa (right), signifying the most important intermolecular contacts. Reproduced with permission from Irii et al.,[232] Copyright 2022, Elsevier.

zo[b,d]thiophene-5,5-dioxide (DBTS) and the closely related, but more rigid carbazole (Cz).[241] Since lattice deformations belong to the softest intramolecular degrees of freedom, DBTS planarizes readily upon pressure application, which leads to a spectroscopic red shift. Cz, on the contrary, is more rigid and rather insensitive to the sterical influence of its surrounding, hence, its absorption and emission spectra are almost unaffected by pressure. In another study, it was observed that conformational changes can turn an expected red shift to a blue shift upon compression.[242]

An important class of piezochromic materials that shall briefly be mentioned here are transition metal complexes. In these cases, the complicated electronic structure poses a formidable challenge to the applied level of theory (cf. Section 3.1.2). DFT has been used to investigate piezochromism in Ir(III),[243,244] Ni(II)[245] and Cu(I)[246] complexes. In the latter case, Energy Decomposition Analysis (EDA)[247] al-

lowed the quantification of important energetic factors, e.g., Pauli repulsion, electrostatic interactions and dispersion, each of which shows complex and system-specific pressure-dependence. In a very recent study, DFT was combined with multireference methods to quantify the effects of energy level changes of electronic states and structural changes on spectroscopic properties of a Cr(III) complex.[248]

Turning to vibrational spectra, high-pressure Raman spectroscopy of chemical compounds is particularly widespread, since Raman spectroscopy on a reference material is typically used anyway to gauge the pressure in a DAC setup. Hence, vibrational properties of molecules under pressure have been calculated fairly early, e.g., in the case of H_2 by applying confining boxes.[76] Later studies using PBC-DFT[249,250] and Quantum Monte Carlo[251] have helped rationalize the existence of the fascinating high-pressure crystal structures of H_2, such as graphene-like sheets.

Due to the importance of vibrations in the rapid degradation mechanism of many explosives and propellants, vibrational properties of energetic materials have been studied extensively, mainly by using (PBC-)DFT.[252] In many cases, a blue shift of the spectroscopic signals was observed.[253,254] However, it must be noted that different vibrational modes react differently to pressure,[255] depending on the precise manner in which the vibrational motions are restricted by the environment, e.g., some vibrational modes in C_{60} that include a high proportion of radial motion are red shifted upon compression.[256] In such cases, intermolecular effects are likely the cause of the observed red shift.

Single-molecule methods have been remarkably successful in reproducing experimental vibrational spectra under pressure. X-HCFF, for example, reproduced the experimentally observed blue shift in the Raman active carbon-hydrogen stretching vibration in the molecular 2-amine-1,3,4-thiadiazole (ATD) crystal.[99] A seminumerical frequency analysis using X-HCFF allowed the characterization of the transition state of a [2,3] sigmatropic (Mislow-Evans) rearrangement and its disappearance at high pressure.[257] XP-PCM was used to calculate intramolecular vibrations and their pressure-induced shifts in sulfur hexafluoride,[258] P_4S_3,[259] C_{60} and C_{70},[256] and diborane,[105] reaching overall good agreement

with experiments. The computational approach subsequently allowed to elucidate the geometrical and energetic basis for the observations.

In a mixed experimental/computational study, DFT using PBCs was used to study the pressure-induced ovalization and aggregation of the [6]cycloparaphenylene ([6]CPP) nanohoop and the resulting Raman spectra.[180] Pressure was observed to cause a blue shift of most Raman modes, but a sudden change in the Raman spectrum was observed at a certain threshold pressure, which was interpreted as a sign of the formation of intermolecular σ bonds on the basis of the DFT calculations. As in many other studies, pressure led to a broadening of Raman modes and to the split of some signals, due to a loss of symmetry in the crystal.

Imoto et al. have demonstrated that AIMD simulations can be used to study high-pressure vibrations.[125] In a study on biomolecular solutions, they have studied pressure-enhanced hydrogen bonding and the resulting infrared response, which has important implications for life in the deep sea. Later it was shown that the computationally less demanding EC-RISM QM/MM method leads to results in good agreement with AIMD and experimental results for the same system.[127]

The vibrational properties of polymeric systems under pressure have been studied by DFT as well, e.g., in polyethylene[260] and the $[Zn(\mu\text{-}Cl)_2(3,5\text{-dichloropyridine})_2]_n$ coordination polymer.[261] In the latter case, it was found that vibrational modes play a role in structural transitions of the polymer.

In summary, piezochromism relies on a complex interplay between intra- and intermolecular effects, which, in many systems, cause opposing trends in the shift of the spectroscopic signal. Experimentally, a net red shift of absorption and luminescence bands is often observed, and reproducing this observation accurately poses a challenge for many computational methods. The behavior of vibrational signals under pressure, on the other hand, is typically easier to reproduce using simulation methods. Many vibrational signals exhibit a blue shift under pressure, which is a result of the shortening of bond lengths and a stiffening of the vibrations. Despite the aforementioned challenges, computational methods have proven

to be indispensable tools for revealing the structural effects underlying the pressure-induced changes in UV/Vis, fluorescence and vibrational spectra.

3.2 Pressure-Induced Chemical Reactions

Pressure gives access to chemical compounds that may be otherwise unobtainable. Hence, the study of high-pressure chemical reactions looks back upon a fascinating history.[10,12] The driving force behind many pressure-induced chemical reactions is the tendency of the compressed systems to minimize their volumes, which can be achieved, e.g., by bond formation.[180]

The identification of transition states at a given pressure is of central importance in studies of high-pressure chemistry, since transition states can be used to calculate reaction barriers. In many cases it was found that transition states become increasingly reactant-like with increasing pressure, and connections with the Hammond postulate have been established.[17] Moreover, the possibility of "trapping" transition states by applying pressure, an approach that was inspired by mechanochemistry,[262,263] has been recently predicted theoretically.[17,257] In the case of high-pressure chemistry, a transition state can potentially be turned into a minimum on the potential energy surface if it occupies a smaller volume than both the reactant and the product of the reaction, which is the case, e.g., in some rearrangement reactions.

In this section, selected simulations of high-pressure chemical reactions are discussed. The focus lies on Diels-Alder reactions (Section 3.2.1) as well as oligomerization and polymerization reactions (Section 3.2.2) under pressure, since numerous computational studies have appeared in these research areas. Finally, the novel concept of the piezomechanical cycle is discussed briefly (Section 3.2.3).

3.2.1 Diels-Alder Reactions

The Diels-Alder reaction is a thermally allowed [4+2] cycloaddition of a diene and a dienophile.[264,265] Due to the mild reaction conditions and the possibility of using a diverse range of reactants, the Diels-

Alder reaction belongs to the most widely used chemical reactions in academia and industry.[266–268] In the realm of high-pressure chemistry, the Diels-Alder reaction has been studied extensively as well: Comprehensive experimental data on reaction and activation volumes and pressure-dependent reaction mechanisms is available.[2,6,269] Changes in reaction volume upon application of experimentally available pressures are significant, ranging between -25 and -40 cm^3/mol.[2] Hence, Diels-Alder reactions are generally accelerated by pressure, which is in good agreement with Le Chatelier's principle and chemical intuition.

Due to the availability of a comprehensive set of experimental reference data, the Diels-Alder reaction under pressure has been scrutinized extensively with *ab initio* simulation techniques. Jha and co-workers, for example, studied the Diels-Alder reaction of butadiene and ethylene at pressures up to 1.4 GPa using G-FMPES in combination with hybrid DFT and multireference wavefunction-based methods.[95] It was found that hydrostatic pressure leads to a lowering of the activation energy barrier and to its eventual disappearance if the pressure is high enough. This finding is in agreement with a recent work on the Diels-Alder reaction of cyclopentadiene and ethylene,[115] in which GOSTSHYP was used to apply pressure both statically *via* DFT and dynamically *via* AIMD simulations. This study demonstrated that low pressure leads to a compression of the van der Waals complex of the reactants before the reaction becomes barrierless at higher pressures. Due to random thermal oscillations, the point in time at which the product is formed at a given pressure is variable.

An impressive body of computational research on pressure-induced Diels-Alder reactions has been produced with XP-PCM. The dimerization reactions of 1,3-cyclohexadiene[270] and cyclopentadiene,[107] respectively, the Diels-Alder reactions of cis-1,2-dihydrocatecholes and electron-deficient electrophiles,[271] cyclopentadiene and ethylene,[17] as well as cylopentadiene and C_{60}[272] have been studied with XP-PCM. Based on these works, some general trends can be deduced: First, pressure decreases the activation energy barrier until it eventually disappears (Figure 8). Second, upon pressure application, the Diels-Alder

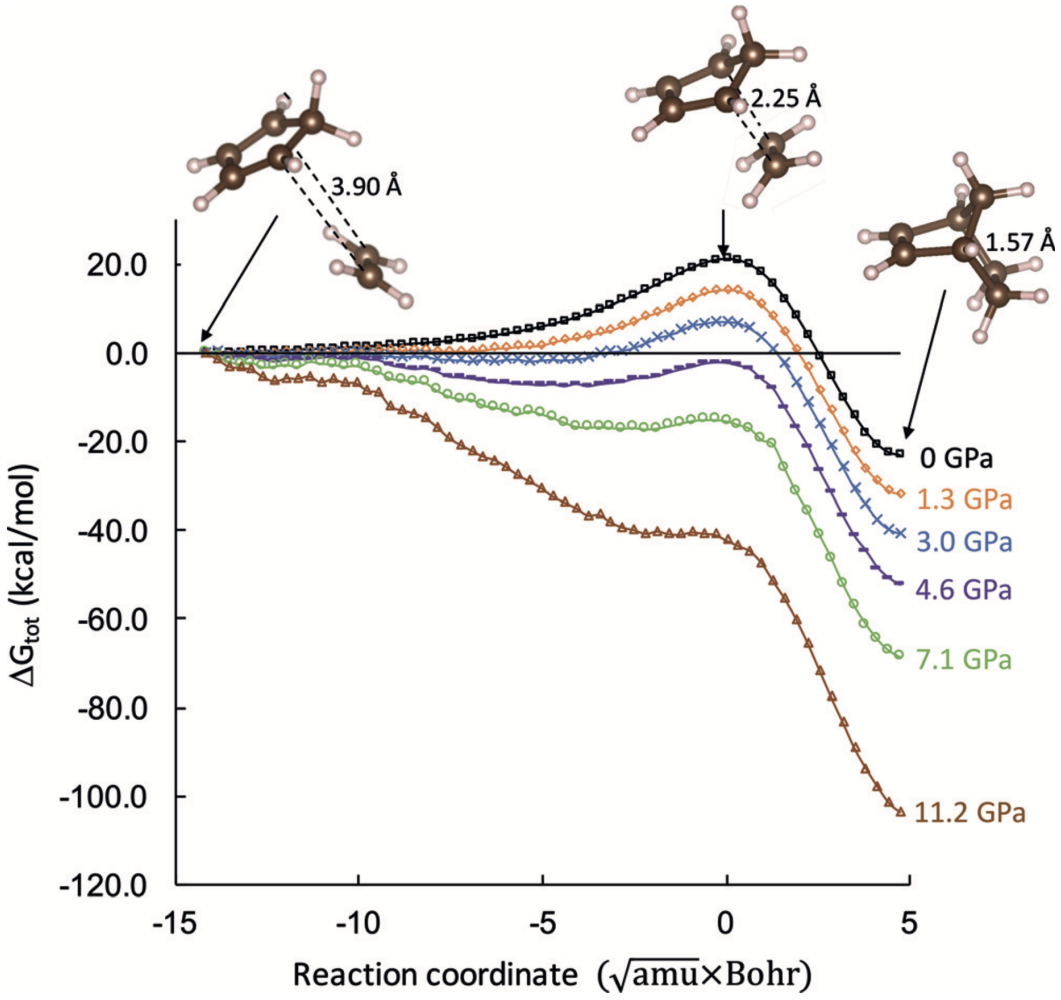

Figure 8: Gibbs free energy profiles of the Diels-Alder reaction of cyclopentadiene and ethylene at different pressures, calculated with XP-PCM. Reproduced with permission from Chen et al.,[270] Copyright 2017, John Wiley and Sons.

reaction becomes more exothermic and the transition state more reactant-like, which agrees with the Hammond postulate. Third, XP-PCM is capable of reproducing experimental activation volumes quite accurately.

The ability of a simulation method to predict activation volumes reliably is valuable, because differences in activation volumes between two otherwise closely related Diels-Alder reactions are a sign of different reaction mechanisms. Hence, a tremendous amount of effort has been devoted to calculating reaction and activation volumes using various models.[273–275] In an early work, for example, Monte Carlo simulation techniques were used on a periodic system to calculate reaction volumes of Diels-Alder reac-

tions.[269] Later, it was demonstrated that MD simulations are capable of reproducing experimental activation volumes (cf. also Section 2.3.2),[120,121] e.g., in the dimerization reaction of cyclopentadiene.[276] Recently, a QM/MM modeling approach allowed the calculation of reaction and activation volumes of the Diels-Alder reaction of cyclopentadiene and acrylonitrile.[277]

These studies demonstrate the power of today's computational tools and their competitiveness with experimental high-pressure techniques. The accurate calculation of reaction and activation volumes, e.g., of Diels-Alder reactions, opens up the possibility to screen a large variety of reactions at the computer and to identify the most promising candidates for later experimental verification. Nevertheless, studies on Diels-Alder reactions under pressure that intimately link experimental and computational techniques are still scarce. In a recent work,[278] PBC-based metadynamics simulations of an azobenzene co-crystal have helped shed light on the reaction mechanisms of competing Diels-Alder ([4+2]) and [2+2] cycloaddition reactions. Moreover, Zholdassov and co-workers recently used a multiscale modeling approach to distinguish between uniaxial stress and hydrostatic compression in a sophisticated nanoreactor setup that induced Diels-Alder reactions between a surface-immobilized anthracene and different dienophiles.[279] Such synergistic studies attest to the usefulness of high-pressure simulation techniques.

We note in passing that the interplay between volume and pressure is crucial for understanding the dissociation mechanism of explosives and propellants. Such systems have been studied with G-FMPES,[96] MD[280] and periodic codes,[281] however, they are not the focus of this review.

3.2.2 From Monomers to Polymers

At high pressure, crystals of organic and molecular inorganic compounds tend to lose their molecular identity. In many cases, an increase in pressure is accompanied by an increase in the number of intermolecular covalent bonds.[282] While this effect grants access to unusual chemical compounds, the possibility of undesired intermolecular bond formation at high pressure needs to be kept in mind as well.

Dimerization is typically the first step towards oligomerization and eventual polymerization of a chemical compound under pressure. A well-known example is the dimerization of cyclopentadiene, which proceeds *via* a [4+2] cycloaddition pathway, but the examples presented in this section go beyond Diels-Alder reactions. Experimentally, a plethora of reactions, ranging from dimerizations to polymerizations, have been observed, e.g., in anthracene,[283] isoprene,[284,285] formic acid,[286] C_{60},[287,288] and butadiene.[289,290] In the latter case, Car-Parrinello Molecular Dynamics (CPMD) simulations have suggested an ionic pathway for the pressure-induced transformation from butadiene to polybutadiene.[291] The finding that pressure leads to an increase in polymerization rate in butadiene is in line with experimental data.[289]

Carbon dioxide (CO_2) has been the target of many computational studies employing high-pressure simulation techniques. Besides the well-founded theoretical and practical interest in the high-pressure behavior of CO_2, the compound has been discussed as a source of carbon in Earth's interior and some relevant chemical reactions have been studied computationally.[292] In an early work,[293] liquid CO_2 was scrutinized with AIMD simulations and the variable-cell method[294] at pressures of up to 50 GPa and temperatures as high as 4000 K. The formation of a metastable dimer with a symmetric four-membered ring was observed at 20 GPa, which remained stable when the pressure was decreased. A similar observation was made with the X-HCFF method,[99] however, CO_2 dimerization was observed at higher pressures than in the aforementioned AIMD simulations (90−100 GPa), which was traced back to the omission of thermal effects in the static X-HCFF calculations. Since thermal oscillations lead to random collisions that may help overcome remaining energy barriers, it can be speculated that static methods based on geometry optimizations at 0 K generally yield higher activation pressures than dynamic methods, e.g., AIMD simulations.

A recent AIMD study[13] allowed the calculation of the phase diagram of CO_2 under Earth mantle conditions (Figure 9). It was found that, below 40 GPa, temperatures above 2000 K are required to make

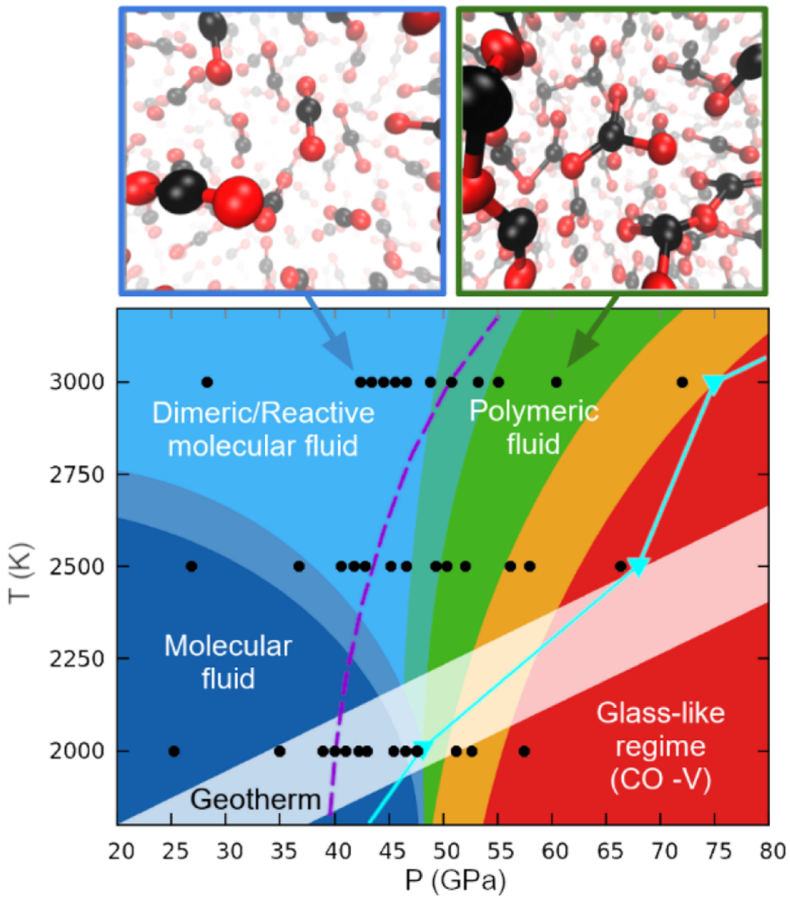

Figure 9: Suggested phase diagram of CO_2 under Earth mantle conditions, based on AIMD simulations. Reproduced with permission from Moog et al.,[13] Copyright 2021, American Chemical Society.

the liquid reactive. At higher pressure, a polymeric fluid was observed. A related SiO_2-like phase was predicted using AIMD early on.[295] Dispersion-corrected DFT using PBCs yielded information on the structure and stability of molecular and non-molecular modifications of CO_2 at high pressure.[296]

Simple boron compounds have been modeled under pressure as well, due to the element's intriguing electronic properties and the ability of a boron atom to form one additional bond. Metadynamics simulations with a supercell of eight BI_3 molecules have yielded a new crystal phase containing dimers of BI_3 with approximate D_{2h} symmetry.[297] The calculated decrease in volume due to the phase transition agrees with experiments. In DFT studies using PBCs, the oligomerization and eventual polymerization of the diborane (B_2H_6) system has been discussed,[298,299] along with a possible metallization if the pressure is high enough.[299]

Moreover, the possibility of unidirectional polymerization of some compounds under pressure has been demonstrated. Consecutive cycloaddition reactions lead to the formation of nanothreads, a futuristic class of one-dimensional polymeric materials valued for their superior mechanical performance.[300–308] Calculations on the pressure-induced synthesis of nanothreads have been performed, e.g., with XP-PCM.[309] The findings of this study are largely in line with those obtained for singular Diels-Alder reactions in that increasing pressure leads to a decrease in volume and activation energy barrier of the cycloadditions. The field of nanothread research, in particular investigations into novel synthetic pathways and the mechanical properties of the materials, will surely continue to grow. It will be exciting to see the crucial contributions made by computational tools in these research endeavors.

3.2.3 The Piezomechanical Cycle

Polymer mechanochemistry is an emerging research area at the intersection between chemistry and materials science,[87,88,310,311] with fascinating applications such as force-triggered release of small molecules[312–316] and the manufacturing of mechanochromic materials.[317–319] At the heart of many functional polymers are mechanophores,[320–324] i.e., molecular constituents of a polymer that respond to stretching forces by significant structural changes, e.g., the rupture of covalent bonds. Typically, mechanophore activation is a one-way process. Once a covalent bond is activated, a desired response is achieved, e.g., a color change in the material or the release of an organic molecule, and restoring a mechanophore to its original form is usually not possible.

However, recently, static X-HCFF calculations and AIMD simulations have demonstrated that hydrostatic pressure can be used for this task.[325] In the iconic spiropyran (SP) mechanophore,[319,326] the force-induced rupture of the central carbon-oxygen bond, which yields merocyanine (MC), can be reverted by hydrostatic pressure in the range of a few GPa (Figure 10). In this process, MC acts as a "piezophore" that responds to pressure by bond formation. As in many pressure-induced chemical reac-

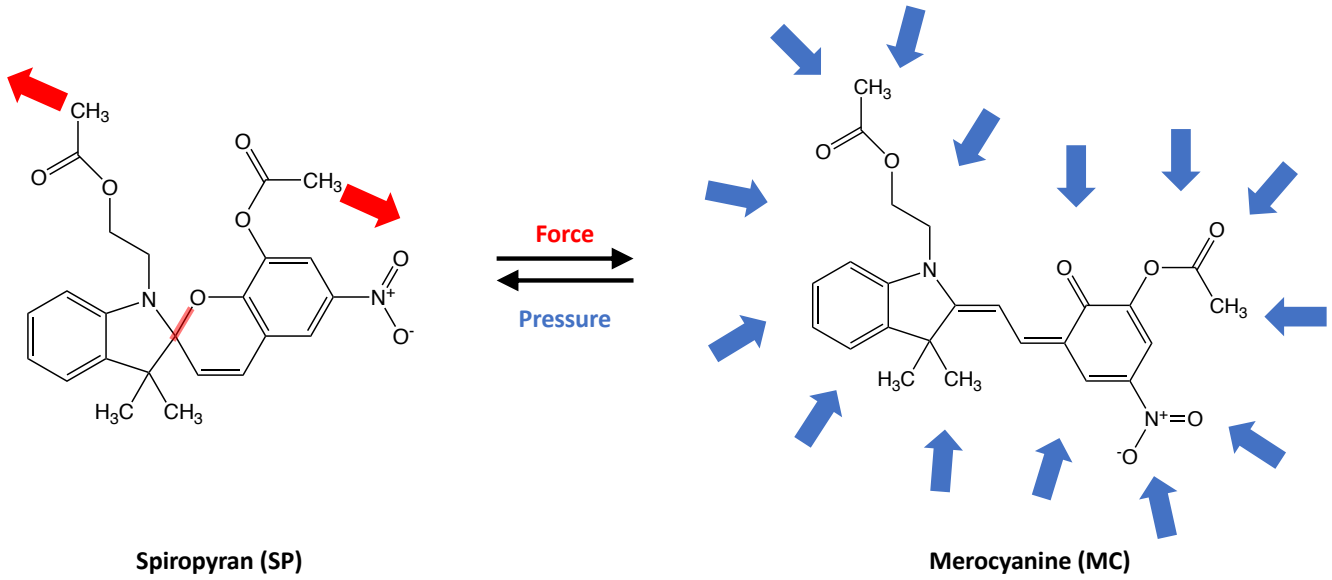

Figure 10: Schematic representation of a piezomechanical cycle, in which the repeated interconversion between spiropyran (SP, left) and merocyanine (MC, right) is triggered by alternating application of mechanical stretching forces and hydrostatic pressure. The scissile carbon-oxygen bond in SP is marked red. Adapted with permission from Kumar et al.,[325] Copyright 2021, American Chemical Society.

tions, the lower volume of SP compared to MC is the driving force for the bond formation reaction. The process of alternating activation of SP by force and of MC by pressure can be repeated several times, thus establishing a piezomechanical (or baromechanical) cycle.

While conceptually promising for the field of polymer mechanochemistry, the piezomechanical cycle has yet to be realized experimentally. The major obstacle to an experimental implementation is that the piezomechanical cycle requires hydrostatic conditions at the molecular level. However, in experiments on (bulk) polymers, realizing such conditions is far from straightforward. On the contrary, pressure is a common way of inducing mechanophore activation[327–331] and the general problem of non-hydrostaticity at the molecular level has been pointed out.[329] In the case of the bisanthracene mechanophore, for example, XP-PCM simulations have helped rationalize pressure-induced bond rupture *via* a leverage principle.[332] To understand mechanical bond cleavage and formation events in functional polymers and the intricate interplay between hydrostatic and anisotropic conditions at the molecular level, multiscale simulation techniques need to be developed and applied to a range of different systems. Such sophisticated

computational tools will allow researchers to exploit the full potential of polymer mechanochemistry and help shed light on the mechanical and high-pressure behavior of molecules embedded in crystals or surrounded by other complex environments.

3.3 The Behavior of Bulk Materials Under Pressure

In this section, we provide some examples of high-pressure simulations of bulk materials, i.e., systems that are typically simulated with periodic boundary conditions (PBC). The focus lies on water, silica melts, hydrogen cyanide, hydrides, carbon-rich materials and biological (macro)molecules under pressure. Metals, semi-conductors and non-molecular crystals, for which a large number of studies exist,[333–338] are not the focus of this review.

As one of the most important molecules for life, it is not surprising that water has been investigated extensively, and the field of computational high-pressure chemistry is no exception. Due to the solidification of water at high pressure, the different phases of ice and their interconversions have been a major focus of computational high-pressure research. For instance, Monte Carlo simulations of the $(H_2O)_{20}$ and $Ar(H_2O)_{20}$ clusters have been conducted to investigate structural transition under high pressure.[339] Changes in the nature of the bonding situation in water due to pressure have been investigated as well, e.g., a DFT study suggested that metallization of ice occurs at 4.7 TPa.[340] As water transitions from low-density to high-density phases, the role of van der Waals (vdW) interactions increases, while the significance of hydrogen bonds decreases.[341,342] Murray and Galli applied DFT with vdW functionals while including the zero point energy contribution and successfully described a wide range of properties of crystalline water under pressure.[343] One key finding of the study was that, at high pressure, the difference in charge densities between low- and high-pressure water is mainly concentrated near the atoms, indicating the weakening of hydrogen bonds at high pressure (Figure 11).

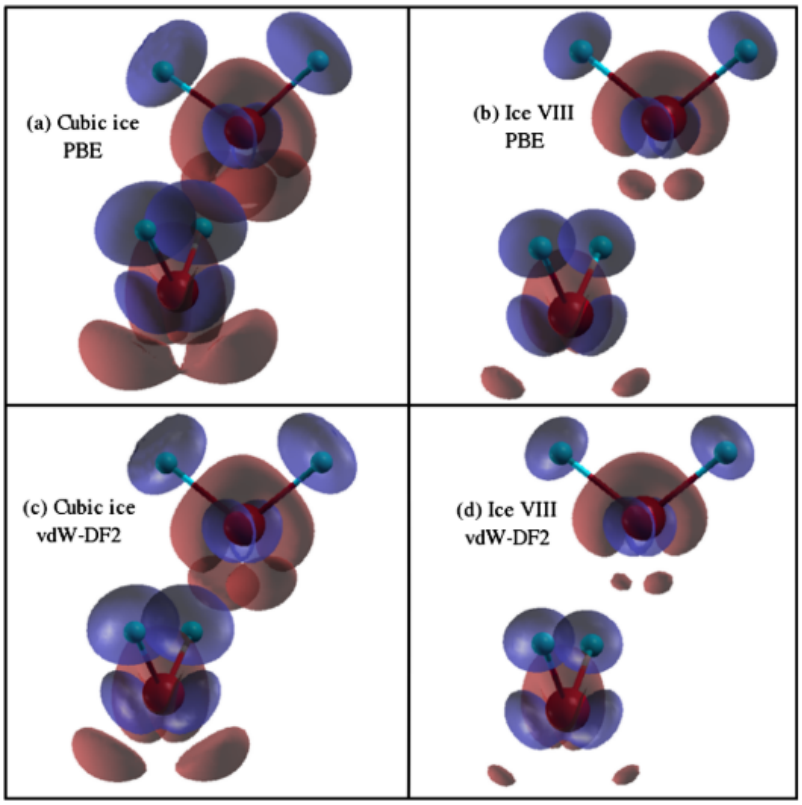

Figure 11: Change in electronic density of cubic ice and ice VIII with respect to the free water molecule, calculated using PBE and vdW-DF2 functionals. The red and blue isosurfaces signify whether the density is increased or decreased, respectively. Oxygen atoms are represented in red, and hydrogen atoms in cyan. Reproduced with permission from Murray and Galli,[343] Copyright 2012, American Physical Society.

The dipole moment of the water molecule changes in response to variations in pressure and temperature. As indicated in an AIMD study by Kang et al.,[344] with increasing temperature, the dipole moment of water decreases due to the collapse of the hydrogen bond network. However, high pressure increases the average dipole moment. Besides, it was found that both high pressure and temperature induce the fluctuation of intramolecular charge, leading to a broader distribution of dipole moments. The observed increase in the dipole moment of water due to pressure agrees with the results obtained *via* single-molecule methods, i.e., wall potentials[75] and GOSTSHYP,[115] which additionally found a reversion of this effect at pressures at several hundred GPa. Finally, AIMD simulations revealed that proton hole (OH^-) migration in water is strongly suppressed at pressures above 10 kbar, but proton (H^+) migration remains unaffected in this pressure range.[345]

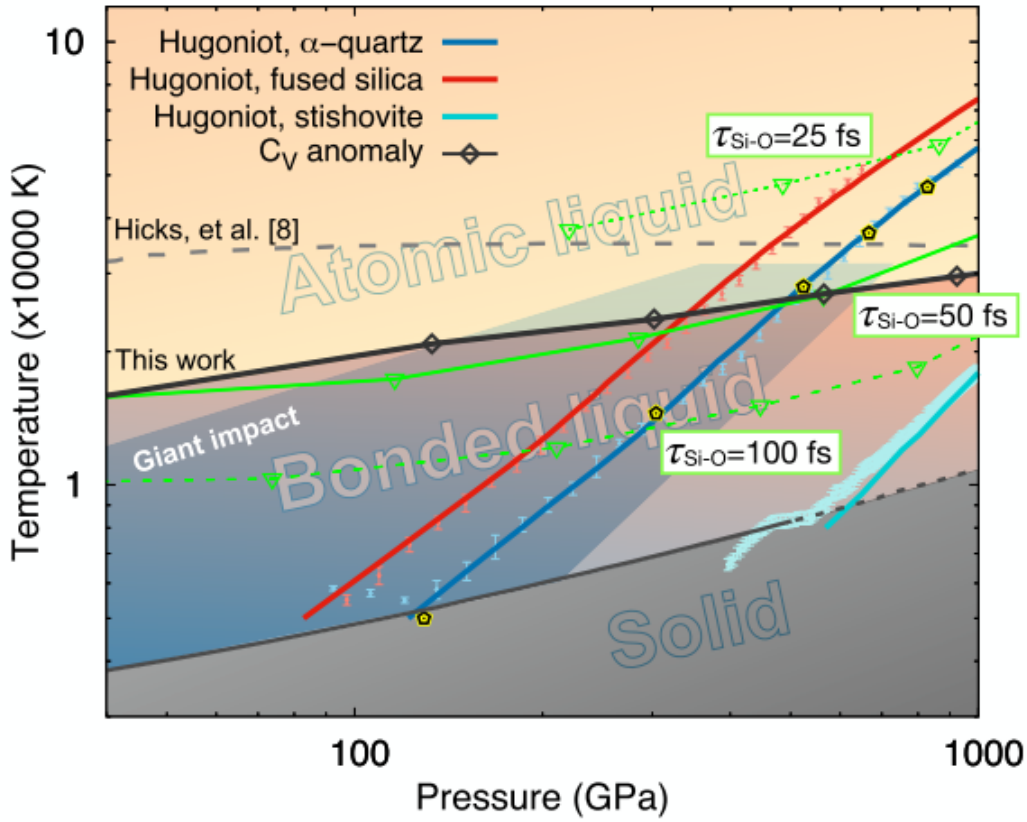

Figure 12: Phase diagram of SiO_2. The black curve with diamond symbols represents the bonded-to-atomic liquid transition found by Zhang et al. Reproduced with permission from Zhang et al.,[349] Copyright 2022, AIP Publishing.

Exploring the properties of silica under high pressure has also gathered interest within the scientific community, as such studies aid our understanding of processes occurring in Earth's mantle. For example, MD simulations of silica melts revealed that the self diffusion coefficient (SDC) of Si and O is pressure-dependent and that fivefold and sixfold coordinated Si sites become widespread under high pressure.[346,347] A study combining MD and high-pressure in situ neutron diffraction indicated that the fivefold coordinated Si sites play a crucial role as intermediates in the transformation of SiO_2 glass from tetrahedral to octahedral coordination under pressure.[348] Zhang et al. investigated silica in the TPa regime by applying MD, thereby explaining the nature of the bond dissociation process in SiO_2 in early Earth and making a contribution to the phase diagram of SiO_2 (Figure 12).[349]

Another system that has been scrutinized under pressure is hydrogen cyanide, which crystallizes

in long chains.[350,351] DFT calculations have revealed that HCN undergoes phase transitions at elevated pressure,[352] and that its high-pressure phases can exhibit insulating, semiconducting, metallic, or ferroelastic behavior.[353,354] Under extreme pressure, HCN polymerizes (cf. Section 3.2.2 for more examples of pressure-induced polymerization processes).[353] Due to the simplicity of the molecular structure and the chain-like geometry of crystalline HCN, this system is suitable for comparing simulations of the full crystal in a PBC setup to model systems with a finite number of molecules. Using X-HCFF and GOST-SHYP it was recently found that simulating a chain with approx. 15-20 HCN molecules reproduces most of the high-pressure structural parameters of a HCN crystal occurring along the crystallographic $\boldsymbol{c}$ axis, i.e., the direction along which the HCN molecules are aligned in the crystal.[185] A similar comparison has been made using XP-PCM in the case of the realgar crystal.[355]

Melicherová and Martoňák studied the polymerization of nitrogen at high pressure and temperature using NPT MD simulations.[356] The authors investigated liquid-liquid and liquid-solid transitions and found that the polymerization of nitrogen at 3000 K takes place between 110 and 115 GPa. With this, the authors achieved better agreement with experimental observations compared to previous studies.[357] This was traced back to the use of a larger simulation cell that allowed chain formation, which might not be possible for smaller cells.

The simplest molecular system, hydrogen, belongs to the most heavily researched elements, and computational studies focusing on its high-pressure liquid[358] and crystalline[359–363] phases are abundant. Soon after the introduction of the Bardeen-Cooper-Schrieffer (BCS) theory in 1957,[364] which describes the phenomenon of superconductivity through electron-phonon coupling, the use of metallic hydrogen as a high-temperature superconductor under high pressure was suggested.[365] A tremendous amount of subsequent research has focused on group IV hydrides, e.g., silane and disilane, as the abundance of hydrogen in these systems makes them "chemically precompressed".[366–368] However, it must be noted that hydrides of various elements are intensively investigated as well.[369–380] Among them, polyhydrides

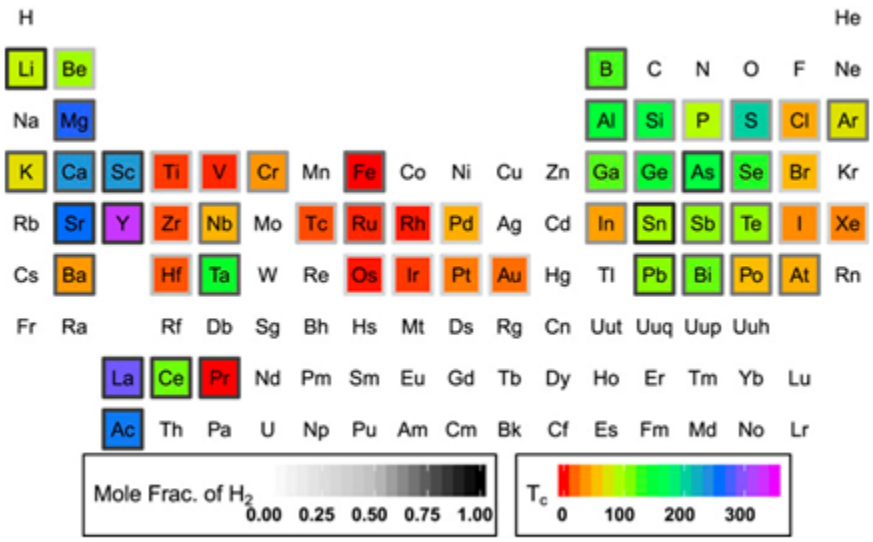

Figure 13: Hydrides of various elements in the periodic table, with color indicating the theoretically predicted superconducting critical temperature T_c (in Kelvin). Gray frames represent the fraction of H_2 in the hydride compound. If an element is not highlighted in color, it signifies that the element is not a hydride superconductor. Reproduced with permission from Zurek and Bi,[381] Copyright 2019, AIP Publishing.

of alkaline earth and rare earth elements generally exhibit high superconducting critical temperature, T_c (Figure 13),[381] i.e., the maximum working temperature for superconductors. Additionally, Zurek and Bi categorized various hydrogenic motifs, among which the clathrate-based hydrogenic lattices, with the metal atom situated at the center of the cages, tend to have high T_c.[381]

The high-pressure properties of carbon-rich materials and their pressure-induced synthesis have been studied extensively as well. A DFT study discovered several high-pressure phases of benzene, including molecular and polymeric phases.[382] The study indicates the stability of polymeric benzene phases owing to the dearomatization of the benzene molecule, involving the breaking of π bonds within the benzene ring and the formation of intermolecular σ bonds. However, it is worth noting that the authors pointed out a substantial energy barrier between the molecular and polymeric benzene phases. Furthermore, a mixed experimental/computational study reported the synthesis of carbon nanothread single crystals from benzene *via* uniaxial compression at room temperature.[383] Carbon allotropes under pressure, e.g.,

graphite,[384] graphene sheets and crystals,[385] and diamond[386] have been intensively studied using diverse simulation techniques. In a recent study, DFT simulations predicted a metallic, superconducting carbon allotrope with significant hardness that could be accessible at high pressure.[387]

The effect of pressure on biological systems is an intriguing topic that shall briefly be mentioned here. While many questions on the biochemical mechanisms of how piezophilic, i.e., pressure-loving, organisms resist pressure remain open, some theories locate the origin of life to deep-sea hydrothermal vents, where early life forms would have been shielded from the harmful radiation of the young sun.[388,389] An early MD study investigated the compressibility and hydration energy of a protein in solution at a pressure of 10 kbar.[390] While this study did not detect any signs of denaturation during the time scale of the simulation, a mixed experimental/MD study revealed structural changes of the human immunodeficiency virus (HIV) protease dimer under high pressure.[391] Song et al. studied the time-dependent elastic properties of cellulose and found that the compressibility, Young's modulus and Poisson's ratio change in response to different deformation rates.[392]

A competing theory attributes the origin of life to high-velocity impacts of astronomical bodies, and MD simulations can provide useful data to support − or contradict − this conjecture. Goldman et al., e.g., applied the *ab initio* MD based multiscale shock compression simulation technique (MSST) to investigate impact-induced shock compression of cometary ice.[393] Cometary ice is primarily composed of water, however, it also contains other molecules such as CO_2, NH_3 and CH_3OH. The results indicate that glycine-containing complexes begin to form after a series of chemical reactions between H^+ ions and transient C-N bonded oligomers, which may have occurred during comet impact events.

4 Conclusions

Modern computational tools allow the simulation of high-pressure structural, electronic and spectroscopic properties of chemical systems of any size and complexity, ranging from single atoms to bulk materials. Pressure-induced crystal structure changes can be predicted, chemical reactions simulated and bonding situations understood. Hence, as in virtually every other branch of chemistry and materials science, computational methods have become invaluable tools that not only complement experiments, but in many cases deliver insights that cannot be derived experimentally. The ability to screen a large variety of chemical systems and pressure-induced transformations computationally allows to extract general principles of high-pressure chemistry without the need to conduct individual, time-consuming experiments.

Nevertheless, it is evident that more synergistic efforts, combining the strengths of both high-pressure experiments and computations, are needed. In such studies, experiments will need to deliver high-quality benchmark data for the applied simulation methods, allowing to test their reliability in reproducing experimental observations and to optimize the computational protocols in return. Dedicated model experiments, as described in Section 2.1.2, will play an important role in this regard. Due to the level of sophistication and the complexity of the experimental setups, it is likely that extensive developmental work in the realm of computational high-pressure chemistry will be carried out throughout the coming decades.

We believe that the development of multiscale high-pressure simulation techniques will become increasingly important in the future. Since the strain applied to a macroscopic object does simply correspond to the strain exerted on the constituent molecules,[394] multiscale models are promising tools to improve the comparability between experiments and calculations. Moreover, the differentiation between isotropic and anisotropic compression is crucial,[27,28] e.g., to gain an understanding why compression can lead to bond rupture at the molecular level.[327–331] Following up on the possibilities for improvement of

high-pressure simulation methods will make sure that the fascinating field of computational high-pressure chemistry continues to thrive.

Funding Information:

We acknowledge financial support through the APF project 'Materials on Demand' within the 'Humans on Mars' Initiative funded by the Federal State of Bremen and the University of Bremen.

Conflict of Interest:

The authors declare no conflict of interest.

References

[1] Katrusiak A. Lab in a DAC - High-pressure Crystal Chemistry in a Diamond-Anvil Cell. Acta Cryst B. 2019;75:918-26.

[2] Schettino V, Bini R. Constraining Molecules at the Closest Approach: Chemistry at High Pressure. Chem Soc Rev. 2007;36:869-80.

[3] McMillan PF. Chemistry at High Pressure. Chem Soc Rev. 2006;35:855-7.

[4] Boldyreva EV. High-Pressure Studies of the Anisotropy of Structural Distortion of Molecular Crystals. J Mol Struct. 2003;647:159-79.

[5] van Eldik R, Klärner FG. High Pressure Chemistry. Synthetic, Mechanistic, and Supercritical Applications. Weinheim: Wiley-VCH; 2002.

[6] Klärner FG, Wurche F. The Effect of Pressure on Organic Reactions. J Prakt Chem. 2000;342(7):609-36.

[7] Klärner FG. Chemie Unter Hochdruck. Chemie Unserer Zeit. 1989;23(2):53-63.

[8] Cammi R, Rahm M, Hoffmann R, Ashcroft NW. Varying Electronic Configurations in Compressed Atoms: From the Role of the Spatial Extension of Atomic Orbitals to the Change of Electronic Configuration as an Isobaric Transformation. J Chem Theory Comput. 2020;16:5047-56.

[9] Rahm M, Cammi R, Ashcroft NW, Hoffmann R. Squeezing All Elements in the Periodic Table: Electron Configuration and Electronegativity of the Atoms under Compression. J Am Chem Soc. 2019;141:10254-71.

[10] Hoffmann R, Hopf H. Learning from Molecules in Distress. Angew Chem Int Ed. 2008;47:4474-81.

[11] Rychkov DA. A Short Review of Current Computational Concepts for High-Pressure Phase Transition Studies in Molecular Crystals. Crystals. 2020 Jan;10(2):81.

[12] Grochala W, Hoffmann R, Feng J, Ashcroft NW. The Chemical Imagination at Work in Very Tight Places. Angew Chem Int Ed. 2007;46:3620-42.

[13] Moog M, Pietrucci F, Saitta AM. Carbon Dioxide under Earth Mantle Conditions: From a Molecular Liquid through a Reactive Fluid to Polymeric Regimes. J Phys Chem A. 2021;125:5863-9.

[14] Weir CE, Lippincott ER, Van Valkenburg A, Bunting EN. Infrared Studies in the 1- to 15-Micron Region to 30,000 Atmospheres. J Res Natl Bur Stan Sect A. 1959 Jul;63A(1):55-62.

[15] Li B, Ji C, Yang W, Wang J, Yang K, Xu R, et al. Diamond Anvil Cell Behavior up to 4 Mbar. Proc Nat Acad Sci USA. 2018;115(8):1713-7.

[16] Stauch T. Quantum Chemical Modeling of Molecules under Pressure. Int J Quantum Chem. 2021;121:e26208.

[17] Chen B, Hoffmann R, Cammi R. The Effect of Pressure on Organic Reactions in Fluids - a New Theoretical Perspective. Angew Chem Int Ed. 2017;56:11126-42.

[18] Hilleke KP, Bi T, Zurek E. Materials under High Pressure: A Chemical Perspective. Appl Phys A. 2022 May;128(5):441.

[19] Miao M, Sun Y, Zurek E, Lin H. Chemistry under High Pressure. Nat Rev Chem. 2020;4(10):508-27.

[20] Goldman N, editor. Computational Approaches for Chemistry Under Extreme Conditions. vol. 28 of Challenges and Advances in Computational Chemistry and Physics. Cham: Springer International Publishing; 2019.

[21] Hoja J, Reilly AM, Tkatchenko A. First-Principles Modeling of Molecular Crystals: Structures and Stabilities, Temperature and Pressure. WIREs Comput Mol Sci. 2017;7:e1294.

[22] Zurek E, Grochala W. Predicting Crystal Structures and Properties of Matter under Extreme Conditions via Quantum Mechanics: The Pressure Is On. Phys Chem Chem Phys. 2015;17(5):2917-34.

[23] Bini R, Schettino V. Materials under Extreme Conditions: Molecular Crystals at High Pressure. London: Imperial College Press; 2014.

[24] Hata H, Nishiyama M, Kitao A. Molecular Dynamics Simulation of Proteins under High Pressure: Structure, Function and Thermodynamics. Biochim Biophys Acta Gen Subj. 2020 Feb;1864(2):129395.

[25] Lin K, Li Q, Yu R, Chen J, Attfield JP, Xing X. Chemical Pressure in Functional Materials. Chem Soc Rev. 2022;51(13):5351-64.

[26] Hauser A, Amstutz N, Delahaye S, Sadki A, Schenker S, Sieber R, et al. Fine Tuning the Electronic Properties of [M(Bpy)3]2+ Complexes by Chemical Pressure (M=Fe2+, Ru2+, Co2+, Bpy=2,2′-Bipyridine). In: Structure and Bonding. vol. 106. Springer Berlin Heidelberg; 2004. p. 81-96.

[27] Zhang R, Cai W, Bi T, Zarifi N, Terpstra T, Zhang C, et al. Effects of Nonhydrostatic Stress on Structural and Optoelectronic Properties of Methylammonium Lead Bromide Perovskite. J Phys Chem Lett. 2017 Aug;8(15):3457-65.

[28] Nagura K, Saito S, Yusa H, Yamawaki H, Fujihisa H, Sato H, et al. Distinct Responses to Mechanical Grinding and Hydrostatic Pressure in Luminescent Chromism of Tetrathiazolylthiophene. J Am Chem Soc. 2013;135:10322-5.

[29] Saslow WM. A History of Thermodynamics: The Missing Manual. Entropy. 2020 Jan;22(1):77.

[30] Michels A, De Boer J, Bijl A. Remarks Concerning Molecular Interaction and Their Influence on the Polarisability. Physica. 1937;4(10):981-94.

[31] Stearn AE, Eyring Henry. Pressure and Rate Processes. Chem Rev. 1941 Dec;29(3):509-23.

[32] Liberman DA. Virial Theorem in Self-Consistent-Field Calculations. Phys Rev B. 1971 Mar;3(6):2081-2.

[33] Tucker TC, Roberts LD, Nestor CW, Carlson TA, Malik FB. Relativistic Self-Consistent-Field Calculation of the Wave Functions, Eigenvalues, Isotope Shifts, and the 6 s Hyperfine-Structure Coupling Constant as a Function of Pressure for Metallic Gold in the Wigner-Seitz Model. Phys Rev. 1969 Feb;178(3):998-1008.

[34] Ludeña EV. SCF Calculations for Hydrogen in a Spherical Box. J Chem Phys. 1977;66:468-70.

[35] Berendsen HJC, Postma JPM, Van Gunsteren WF, Dinola A, Haak JR. Molecular Dynamics with Coupling to an External Bath. J Chem Phys. 1984;81:3684-90.

[36] Nosé S, Klein ML. Constant Pressure Molecular Dynamics for Molecular Systems. Mol Phys. 1983;50(5):1055-76.

[37] Parrinello M, Rahman A. Polymorphic Transitions in Single Crystals: A New Molecular Dynamics Method. J Appl Phys. 1981;52:7182-90.

[38] Andersen HC. Molecular Dynamics Simulations at Constant Pressure and/or Temperature. J Chem Phys. 1980 Feb;72(4):2384-93.

[39] Nielsen OH, Martin RM. First-Principles Calculation of Stress. Phys Rev Lett. 1983 Feb;50(9):697-700.

[40] Hartree DR. The Wave Mechanics of an Atom with a Non-Coulomb Central Field. Math Proc Camb Philos Soc. 1928;24(1):111-32.

[41] Hartree DR, Hartree W. Self-Consistent Field, with Exchange, for Beryllium. Proc Royal Soc Lond A. 1935;150:9-33.

[42] Møller C, Plesset MS. Note on an Approximation Treatment for Many-Electron Systems. Phys Rev. 1934;46:618-22.

[43] Coester F, Kümmel H. Short-Range Correlations in Nuclear Wave Functions. Nucl Phys. 1960;17:477-85.

[44] Purvis III GD, Bartlett RJ. A Full Coupled-Cluster Singles and Doubles Model: The Inclusion of Disconnected Triples. J Chem Phys. 1982;76:1910-8.

[45] Raghavachari K, Trucks GW, Pople JA, Head-Gordon M. A Fifth-Order Perturbation Comparison of Electron Correlation Theories. Chem Phys Lett. 1989;157(6):479-83.

[46] Adler TB, Werner HJ. Local Explicitly Correlated Coupled-Cluster Methods: Efficient Removal of the Basis Set Incompleteness and Domain Errors. J Chem Phys. 2009 Jun;130(24):241101.

[47] Knizia G, Adler TB, Werner HJ. Simplified CCSD(T)-F12 Methods: Theory and Benchmarks. J Chem Phys. 2009 Feb;130(5):054104.

[48] Riplinger C, Neese F. An Efficient and near Linear Scaling Pair Natural Orbital Based Local Coupled Cluster Method. J Chem Phys. 2013 Jan;138(3):034106.

[49] Riplinger C, Sandhoefer B, Hansen A, Neese F. Natural Triple Excitations in Local Coupled Cluster Calculations with Pair Natural Orbitals. J Chem Phys. 2013 Oct;139(13):134101.

[50] Riplinger C, Pinski P, Becker U, Valeev EF, Neese F. Sparse Maps—A Systematic Infrastructure for Reduced-Scaling Electronic Structure Methods. II. Linear Scaling Domain Based Pair Natural Orbital Coupled Cluster Theory. J Chem Phys. 2016 Jan;144(2):024109.

[51] Sahraoui B, Kityk IV, Phu XN, Hudhomme P, Gorgues A. Influence of Hydrostatic Pressure and Temperature on Two-Photon Absorption of a C60-2-thioxo-1,3-Dithole Cycloadduct. Phys Rev B. 1999;59(14):9229-38.

[52] Geerlings P, De Proft F. External Fields in Conceptual Density Functional Theory. J Comput Chem. 2023 Jan;44(3):442-55.

[53] Francotte R, Irons TJP, Teale AM, De Proft F, Geerlings P. Extending Conceptual DFT to Include External Variables: The Influence of Magnetic Fields. Chem Sci. 2022;13(18):5311-24.

[54] Sauer J, Freund HJ. Models in Catalysis. Catal Lett. 2015 Jan;145(1):109-25.

[55] McWilliams RS, Spaulding DK, Eggert JH, Celliers PM, Hicks DG, Smith RF, et al. Phase Transformations and Metallization of Magnesium Oxide at High Pressure and Temperature. Science. 2012 Dec;338(6112):1330-3.

[56] Holmström E, Stixrude L. Spin Crossover in Liquid (Mg,Fe)O at Extreme Conditions. Phys Rev B. 2016 May;93(19):195142.

[57] Sommerfeld A, Welker H. Künstliche Grenzbedingungen beim Keplerproblem. Ann Phys. 1938 Jan;424(1-2):56-65.

[58] Connerade JP. Confining and Compressing the Atom. Eur Phys J D. 2020 Oct;74(10):211.

[59] Sabin JR, Brändas EJ. Advances in Quantum Chemistry. Theory of Confined Quantum Systems - Part One. 1st ed. Academic Press; 2009.

[60] Sabin JR, Brändas EJ. Advances in Quantum Chemistry. Theory of Confined Quantum Systems - Part Two. 1st ed. Academic Press; 2009.

[61] Aquino N, Campoy G, Montgomery Jr HE. Highly Accurate Solutions for the Confined Hydrogen Atom. Int J Quantum Chem. 2007 Jan;107(7):1548-58.

[62] Burrows BL, Cohen M. Exact Solutions for Perturbed Confined Hydrogen Atoms: Polarizabilities and Nuclear Shielding Factors. Phys Rev A. 2005 Sep;72(3):032508.

[63] Montgomery HE. Dynamic Dipole Polarizabilities of the Confined Hydrogen Atom. Chem Phys Lett. 2002 Feb;352(5-6):529-32.

[64] Goldman S, Joslin C. Spectroscopic Properties of an Isotropically Compressed Hydrogen Atom. J Phys Chem. 1992 Jul;96(14):6021-7.

[65] Suryanarayana D, Weil JA. On the Hyperfine Splitting of the Hydrogen Atom in a Spherical Box. J Chem Phys. 1976;64(2):510-3.

[66] De Groot SR, Ten Seldam CA. On the Energy Levels of a Model of the Compressed Hydrogen Atom. Physica. 1946 Dec;12(9-10):669-82.

[67] Burrows BL, Cohen M. Exact Solutions for Spherically Confined Hydrogen-like Atoms. Int J Quantum Chem. 2006 Jan;106(2):478-84.

[68] Ley-Koo E, Cruz SA. The Hydrogen Atom and the H+2 and HeH++ Molecular Ions inside Prolate Spheroidal Boxes. J Chem Phys. 1981 Apr;74(8):4603-10.

[69] Robles-Navarro A, Cárdenas C, Fuentealba P. Electronegativity under Confinement. Molecules. 2021;26:6924.

[70] Montgomery Jr HE, Aquino N, Flores-Riveros A. The Ground State Energy of a Helium Atom under Strong Confinement. Phys Lett A. 2010 Apr;374(19-20):2044-7.

[71] Gorecki J, Byers Brown W. On the Ground State of the Hydrogen Molecule-Ion H2+ Enclosed in Hard and Soft Spherical Boxes. J Chem Phys. 1988;89:2138-48.

[72] Gray BF, Gonda I. Application of Rayleigh–Schrödinger Perturbation Theory to the Hydrogen Atom. III. J Chem Phys. 1975 Mar;62(5):2007-8.

[73] Varshni YP. Accurate Wavefunctions for the Confined Hydrogen Atom at High Pressures. J Phys B: At Mol Opt Phys. 1997 Sep;30(18):L589-93.

[74] Waugh S, Chowdhury A, Banerjee A. On the Variation of Polarizability and Hyperpolarizability of a Confined Atom with the Strength of Confinement: A Case Study of a Helium Atom. J Phys B: At Mol Opt Phys. 2010 Nov;43(22):225002.

[75] Cruz SA, Soullard J. Pressure Effects on the Electronic and Structural Properties of Molecules. Chem Phys Lett. 2004;391:138-42.

[76] LeSar R, Herschbach DR. Electronic and Vibrational Properties of Molecules at High Pressures. Hydrogen Molecule in a Rigid Spheroidal Box. J Chem Phys. 1981;85:2798-804.

[77] Ten Seldam CA, De Groot SR. On the Ground State of a Model for Compressed Helium. Physica. 1952 Nov;18(11):891-904.

[78] Cottrell TL. Molecular Energy at High Pressure. Transactions of the Faraday Society. 1951;47:337-42.

[79] Ley-Koo E, Rubinstein S. The Hydrogen Atom within Spherical Boxes with Penetrable Walls. J Chem Phys. 1979;71:351-7.

[80] Katriel J, Montgomery Jr HE. The Virial Theorem for the Smoothly and Sharply, Penetrably and Impenetrably Confined Hydrogen Atom. J Chem Phys. 2012 Sep;137(11):114109.

[81] Bielińska-Waż D, Diercksen GHF, Klobukowski M. Quantum Chemistry of Confined Systems: Structure and Vibronic Spectra of a Confined Hydrogen Molecule. Chem Phys Lett. 2001;349:215-9.

[82] Bielińska-Waż D, Karwowski J, Diercksen GHF. Spectra of Confined Two-Electron Atoms. J Phys B: At Mol Opt Phys. 2001 May;34(10):1987-2000.

[83] Pašteka LF, Helgaker T, Saue T, Sundholm D, Werner HJ, Hasanbulli M, et al. Atoms and Molecules in Soft Confinement Potentials. Mol Phys. 2020;118:e1730989.

[84] Fernández FM, Castro EA. Virial Theorem and Boundary Conditions for Approximate Wave Functions. Int J Quantum Chem. 1982 Apr;21(4):741-51.

[85] Bader RFW, Austen MA. Properties of Atoms in Molecules: Atoms under Pressure. J Chem Phys. 1997;107(11):4271-85.

[86] Beyer MK, Clausen-Schaumann H. Mechanochemistry: The Mechanical Activation of Covalent Bonds. Chem Rev. 2005;105:2921-48.

[87] Ribas-Arino J, Marx D. Covalent Mechanochemistry: Theoretical Concepts and Computational Tools with Applications to Molecular Nanomechanics. Chem Rev. 2012;112:5412-87.

[88] Stauch T, Dreuw A. Advances in Quantum Mechanochemistry: Electronic Structure Methods and Force Analysis. Chem Rev. 2016;116:14137-80.

[89] Levitas VI. High-Pressure Mechanochemistry: Conceptual Multiscale Theory and Interpretation of Experiments. Phys Rev B. 2004 Nov;70(18):184118.

[90] Beyer MK. The Mechanical Strength of a Covalent Bond Calculated by Density Functional Theory. J Chem Phys. 2000;112(17):7307-12.

[91] Ribas-Arino J, Shiga M, Marx D. Understanding Covalent Mechanochemistry. Angew Chem Int Ed. 2009;48:4190-3.

[92] Ong MT, Leiding J, Tao H, Virshup AM, Martínez TJ. First Principles Dynamics and Minimum Energy Pathways for Mechanochemical Ring Opening of Cyclobutene. J Am Chem Soc. 2009;131:6377-9.

[93] Wolinski K, Baker J. Theoretical Predictions of Enforced Structural Changes in Molecules. Mol Phys. 2009;107(22):2403-17.

[94] Subramanian G, Mathew N, Leiding J. A Generalized Force-Modified Potential Energy Surface for Mechanochemical Simulations. J Chem Phys. 2015;143:134109.

[95] Jha SK, Brown K, Todde G, Subramanian G. A Mechanochemical Study of the Effects of Compression on a Diels-Alder Reaction. J Chem Phys. 2016;145:074307.

[96] Todde G, Jha SK, Subramanian G. The Effect of External Forces on the Initial Dissociation of RDX (1,3,5-Trinitro-1,3,5-Triazine): A Mechanochemical Study. Int J Quantum Chem. 2017;117:e25426.

[97] Stauch T, Chakraborty R, Head-Gordon M. Quantum Chemical Modeling of Pressure-Induced Spin Crossover in Octahedral Metal-Ligand Complexes. ChemPhysChem. 2019;20:2742-7.

[98] Lange AW, Herbert JM. Polarizable Continuum Reaction-Field Solvation Models Affording Smooth Potential Energy Surfaces. J Phys Chem Lett. 2010;1:556-61.

[99] Stauch T. A Mechanochemical Model for the Simulation of Molecules and Molecular Crystals under Hydrostatic Pressure. J Chem Phys. 2020;153:134503.

[100] Epifanovsky E, Gilbert ATB, Feng X, Lee J, Mao Y, Mardirossian N, et al. Software for the Frontiers of Quantum Chemistry: An Overview of Developments in the Q-Chem 5 Package. J Chem Phys. 2021;155:084801.

[101] Tomasi J. Selected Features of the Polarizable Continuum Model for the Representation of Solvation. WIREs Comput Mol Sci. 2011 Sep;1(5):855-67.

[102] Mennucci B. Polarizable Continuum Model. WIREs Comput Mol Sci. 2012 May;2(3):386-404.

[103] Herbert JM. Dielectric Continuum Methods for Quantum Chemistry. WIREs Comput Mol Sci. 2021 Jul;11(4):e1519.

[104] Cammi R, Verdolino V, Mennucci B, Tomasi J. Towards the Elaboration of a QM Method to Describe Molecular Solutes under the Effect of a Very High Pressure. Chem Phys. 2008;344:135-41.

[105] Cammi R, Cappelli C, Mennucci B, Tomasi J. Calculation and Analysis of the Harmonic Vibrational Frequencies in Molecules at Extreme Pressure: Methodology and Diborane as a Test Case. J Chem Phys. 2012;137:154112.

[106] Fukuda R, Ehara M, Cammi R. Modeling Molecular Systems at Extreme Pressure by an Extension of the Polarizable Continuum Model (PCM) Based on the Symmetry-Adapted Cluster-Configuration Interaction (SAC-CI) Method: Confined Electronic Excited States of Furan as a Test Case. J Chem Theory Comput. 2015;11:2063-76.

[107] Cammi R. A New Extension of the Polarizable Continuum Model: Toward a Quantum Chemical Description of Chemical Reactions at Extreme High Pressure. J Comput Chem. 2015;36:2246-59.

[108] Cammi R. The Quantum Chemical Study of Chemical Reactions at Extreme High Pressure by Means of the Extreme-Pressure Polarizable Continuum Model. In: Annu. Rep. Comput. Chem.. vol. 13. Elsevier B.V.; 2017. p. 117-35.

[109] Cammi R, Chen B, Rahm M. Analytical Calculation of Pressure for Confined Atomic and Molecular Systems Using the eXtreme-Pressure Polarizable Continuum Model. J Comput Chem. 2018;39:2243-50.

[110] Cammi R. Quantum Chemistry at the High Pressures: The eXtreme Pressure Polarizable Continuum Model (XP-PCM). In: Wójcik MJ, Nakatsuji H, Kirtman B, Ozaki Y, editors. Frontiers of Quantum Chemistry. Springer; 2018. p. 273-88.

[111] Gale A, Hruska E, Liu F. Quantum Chemistry for Molecules at Extreme Pressure on Graphical Processing Units: Implementation of Extreme-Pressure Polarizable Continuum Model. J Chem Phys. 2021 Jun;154(24):244103.

[112] Cammi R, Chen B. The Second Derivative of the Electronic Energy with Respect to the Compression Scaling Factor in the XP-PCM Model : Theory and Applications to Compression Response Functions of Atoms. J Comput Chem. 2022:DOI: 10.1002/jcc.26883.

[113] Cammi R, Chen B. Studying and Exploring Potential Energy Surfaces of Compressed Molecules: A Fresh Theory from the eXtreme Pressure Polarizable Continuum Model. J Chem Phys. 2022 Aug;157:114101.

[114] Eeckhoudt J, Bettens T, Geerlings P, Cammi R, Chen B, Alonso M, et al. Conceptual Density Functional Theory under Pressure: Part I. XP-PCM Method Applied to Atoms. Chem Sci. 2022;13(32):9329-50.

[115] Scheurer M, Dreuw A, Epifanovsky E, Head-Gordon M, Stauch T. Modeling Molecules under Pressure with Gaussian Potentials. J Chem Theory Comput. 2021;17:583-97.

[116] Zeller F, Berquist E, Epifanovsky E, Neudecker T. An Efficient Implementation of the GOSTSHYP Pressure Model by Applying Shell-Bounding Gaussian 1-Electron-3-Center Integral Screening. J Chem Phys. 2022;157:184802.

[117] Labet V, Hoffmann R, Ashcroft NW. A Fresh Look at Dense Hydrogen under Pressure. II. Chemical and Physical Models Aiding Our Understanding of Evolving H–H Separations. J Chem Phys. 2012;136(7):074502.

[118] Miao MS, Hoffmann R. High Pressure Electrides: A Predictive Chemical and Physical Theory. Acc Chem Res. 2014 Apr;47(4):1311-7.

[119] Dong X, Oganov AR, Cui H, Zhou XF, Wang HT. Electronegativity and Chemical Hardness of Elements under Pressure. Proc Natl Acad Sci USA. 2022 Mar;119(10):e2117416119.

[120] Wiebe H, Spooner J, Boon N, Deglint E, Edwards E, Dance P, et al. Calculation of Molecular Volumes and Volumes of Activation Using Molecular Dynamics Simulations. J Phys Chem C. 2012;116:2240-5.

[121] Spooner J, Wiebe H, Boon N, Deglint E, Edwards E, Yanciw B, et al. Molecular Dynamics Calculation of Molecular Volumes and Volumes of Activation. Phys Chem Chem Phys. 2012;14(7):2264.

[122] Spooner J, Yanciw B, Wiebe B, Weinberg N. Reaction Profiles and Energy Surfaces of Compressed Species. J Phys Chem A. 2014;118:765-77.

[123] Kloss T, Heil J, Kast SM. Quantum Chemistry in Solution by Combining 3D Integral Equation Theory with a Cluster Embedding Approach. J Phys Chem B. 2008 Apr;112(14):4337-43.

[124] Hölzl C, Kibies P, Imoto S, Frach R, Suladze S, Winter R, et al. Design Principles for High–Pressure Force Fields: Aqueous TMAO Solutions from Ambient to Kilobar Pressures. J Chem Phys. 2016 Apr;144(14):144104.

[125] Imoto S, Kibies P, Rosin C, Winter R, Kast SM, Marx D. Toward Extreme Biophysics: Deciphering the Infrared Response of Biomolecular Solutions at High Pressures. Angew Chem Int Ed. 2016;55:9534-8.

[126] Frach R, Kibies P, Böttcher S, Pongratz T, Strohfeldt S, Kurrmann S, et al. The Chemical Shift Baseline for High-Pressure NMR Spectra of Proteins. Angew Chem Int Ed. 2016 Jul;55(30):8757-60.

[127] Pongratz T, Kibies P, Eberlein L, Tielker N, Hölzl C, Imoto S, et al. Pressure-Dependent Electronic Structure Calculations Using Integral Equation-Based Solvation Models. Biophys Chem. 2020 Feb;257:106258.

[128] Sode O, Hirata S. Second-Order Many-Body Perturbation Study of Solid Hydrogen Fluoride under Pressure. Phys Chem Chem Phys. 2012;14(21):7765.

[129] Sode O, Hirata S. Second-Order Many-Body Perturbation Study of Solid Hydrogen Fluoride. J Phys Chem A. 2010 Aug;114(33):8873-7.

[130] Gordon MS, Fedorov DG, Pruitt SR, Slipchenko LV. Fragmentation Methods: A Route to Accurate Calculations on Large Systems. Chem Rev. 2012 Jan;112(1):632-72.

[131] Hirata S, Gilliard K, He X, Li J, Sode O. Ab Initio Molecular Crystal Structures, Spectra, and Phase Diagrams. Acc Chem Res. 2014 Sep;47(9):2721-30.

[132] Han Y, Liu J, Li J. Molecular Structure Determination of Solid Carbon Dioxide Phase IV at High Pressures and Temperatures Based on Møller-Plesset Perturbation Theory. Int J Quantum Chem. 2020 Dec;120(23):e26397.

[133] Han Y, Liu J, Huang L, He X, Li J. Predicting the Phase Diagram of Solid Carbon Dioxide at High Pressure from First Principles. npj Quantum Mater. 2019 Mar;4(1):10.

[134] Xiao R, Huang L, Han Y, Liu J, Li J. Ab Initio Phase Transition Prediction for Ices XV/XIV/VIII at High Pressures and Low Temperatures. Chem Phys Lett. 2020 Dec;760:138015.

[135] Salim MA, Willow SY, Hirata S. Ice Ih Anomalies: Thermal Contraction, Anomalous Volume Isotope Effect, and Pressure-Induced Amorphization. J Chem Phys. 2016 May;144(20):204503.

[136] Wang Y, Ma Y. Perspective: Crystal Structure Prediction at High Pressures. J Chem Phys. 2014 Jan;140(4):040901.

[137] Bloch F. Uber die Quantenmechanik der Elektronen in Kristallgittern. Z Phys. 1929;52:555-600.

[138] Blöchl PE. Projector Augmented-Wave Method. Phys Rev B. 1994;50(24):17953-79.

[139] Nielsen OH, Martin RM. Quantum-Mechanical Theory of Stress and Force. Phys Rev B. 1985 Sep;32(6):3780-91.

[140] Nielsen OH, Martin RM. Stresses in Semiconductors: Ab Initio Calculations on Si, Ge, and GaAs. Phys Rev B. 1985 Sep;32(6):3792-805.

[141] Ehrenfest P. Bemerkung Über Die Angenäherte Gültigkeit Der Klassischen Mechanik Innerhalb Der Quantenmechanik. Z Phys. 1927;45:455-7.

[142] Born M, Heisenberg W, Jordan P. Zur Quantenmechanik. II. Z Phys. 1926;35:557-615.

[143] Finkelstein BN. Über Den Virialsatz in Der Wellenmechanik. Z Phys. 1928;50:293-4.

[144] Hylleraas EA. Neue Berechnung der Energie des Heliums im Grundzustande, sowie des tiefsten Terms von Ortho-Helium. Z Phys. 1929 May;54(5-6):347-66.

[145] Fock V. Bemerkung zum Virialsatz. Z Phys. 1930 Nov;63(11-12):855-8.

[146] Slater JC. The Virial and Molecular Structure. J Chem Phys. 1933 Oct;1(10):687-91.

[147] Bidault X, Chaudhuri S. Improved Predictions of Thermomechanical Properties of Molecular Crystals from Energy and Dispersion Corrected DFT. J Chem Phys. 2021;154:164105.

[148] Otero-de-la-Roza A, Luaña V. Equations of State and Thermodynamics of Solids Using Empirical Corrections in the Quasiharmonic Approximation. Phys Rev B. 2011 Nov;84(18):184103.

[149] Hummer G, Grønbech-Jensen N, Neumann M. Pressure Calculation in Polar and Charged Systems Using Ewald Summation: Results for the Extended Simple Point Charge Model of Water. The Journal of Chemical Physics. 1998 Aug;109(7):2791-7.

[150] Louwerse MJ, Baerends EJ. Calculation of Pressure in Case of Periodic Boundary Conditions. Chem Phys Lett. 2006;421:138-41.

[151] Thompson AP, Plimpton SJ, Mattson W. General Formulation of Pressure and Stress Tensor for Arbitrary Many-Body Interaction Potentials under Periodic Boundary Conditions. J Chem Phys. 2009;131:154107.

[152] Hoover WG. Constant-Pressure Equations of Motion. Phys Rev A. 1986;34(3):2499-500.

[153] Wentzcovitch RM. Invariant Molecular-Dynamics Approach to Structural Phase Transitions. Phys Rev B. 1991;44(5):2358-61.

[154] Faller R, De Pablo JJ. Constant Pressure Hybrid Molecular Dynamics–Monte Carlo Simulations. J Chem Phys. 2002 Jan;116(1):55-9.

[155] Åqvist J, Wennerström P, Nervall M, Bjelic S, Brandsdal BO. Molecular Dynamics Simulations of Water and Biomolecules with a Monte Carlo Constant Pressure Algorithm. Chem Phys Lett. 2004 Jan;384(4-6):288-94.

[156] Wiebke J, Pahl E, Schwerdtfeger P. Melting at High Pressure: Can First-Principles Computational Chemistry Challenge Diamond-Anvil Cell Experiments? Angew Chem Int Ed. 2013;52(50):13202-5.

[157] Steele BA, Goldman N, Kuo IFW, Kroonblawd MP. Mechanochemical Synthesis of Glycine Oligomers in a Virtual Rotational Diamond Anvil Cell. Chem Sci. 2020;11:7760-71.

[158] Hasnip PJ, Refson K, Probert MIJ, Yates JR, Clark SJ, Pickard CJ. Density Functional Theory in the Solid State. Phil Trans R Soc A. 2014 Mar;372(2011):20130270.

[159] Giustino F. Materials Modelling Using Density Functional Theory: Properties and Predictions. Oxford University Press; 2014.

[160] Hafner J. Ab-Initio Simulations of Materials Using VASP: Density-functional Theory and Beyond. J Comput Chem. 2008 Oct;29(13):2044-78.

[161] Hammouri M, Garcia TM, Cook C, Monaco S, Jezowski S, Marom N, et al. High-Throughput Pressure-Dependent Density Functional Theory Investigation of Herringbone Polycyclic Aromatic Hydrocarbons: Part 1. Pressure-Dependent Structure Trends. J Phys Chem C. 2018 Oct;122(42):23815-27.

[162] Hammouri M, Garcia TM, Cook C, Monaco S, Jezowski S, Marom N, et al. High-Throughput Pressure-Dependent Density Functional Theory Investigation of Herringbone Polycyclic Aromatic Hydrocarbons: Part 2. Pressure-Dependent Electronic Properties. J Phys Chem C. 2018 Oct;122(42):23828-44.

[163] Rahm M, Ångqvist M, Rahm JM, Erhart P, Cammi R. Non-Bonded Radii of the Atoms Under Compression. ChemPhysChem. 2020;21:2441-53.

[164] Rahm M, Erhart P, Cammi R. Relating Atomic Energy, Radius and Electronegativity through Compression. Chem Sci. 2021;12(7):2397-403.

[165] Feng J, Hennig RG, Ashcroft NW, Hoffmann R. Emergent Reduction of Electronic State Dimensionality in Dense Ordered Li-Be Alloys. Nature. 2008 Jan;451(7177):445-8.

[166] Rahm M. Electronegativity at the Shock Front. Propellants Explos Pyrotech. 2023;48:e202100306.

[167] Geerlings P, De Proft F, Langenaeker W. Conceptual Density Functional Theory. Chem Rev. 2003 May;103(5):1793-874.

[168] Sarsa A, Alcaraz-Pelegrina JM, Le Sech C. Exclusion Principle Repulsion Effects on the Covalent Bond beyond the Born–Oppenheimer Approximation. Phys Chem Chem Phys. 2019;21(20):10411-6.

[169] Miao M, Sun Y, Liu H, Ma Y. Open Questions on the High-Pressure Chemistry of the Noble Gases. Commun Chem. 2022 Feb;5(1):15.

[170] Liu Z, Botana J, Hermann A, Valdez S, Zurek E, Yan D, et al. Reactivity of He with Ionic Compounds under High Pressure. Nat Commun. 2018 Mar;9(1):951.

[171] Zarifi N, Liu H, Tse JS, Zurek E. Crystal Structures and Electronic Properties of Xe–Cl Compounds at High Pressure. J Phys Chem C. 2018 Feb;122(5):2941-50.

[172] Hermann A, Schwerdtfeger P. Xenon Suboxides Stable under Pressure. J Phys Chem Lett. 2014 Dec;5(24):4336-42.

[173] Grochala W. Atypical Compounds of Gases, Which Have Been Called 'Noble'. Chem Soc Rev. 2007;36:1632-55.

[174] Yoo CS. Chemistry under Extreme Conditions: Pressure Evolution of Chemical Bonding and Structure in Dense Solids. Matter Radiat at Extremes. 2020 Jan;5(1):018202.

[175] Kurzydłowski D, Zaleski-Ejgierd P, Grochala W, Hoffmann R. Freezing in Resonance Structures for Better Packing: XeF_2 Becomes $(XeF^+)(F^-)$ at Large Compression. Inorg Chem. 2011 Apr;50(8):3832-40.

[176] Sperling JM, Warzecha EJ, Celis-Barros C, Sergentu DC, Wang X, Klamm BE, et al. Compression of Curium Pyrrolidine-Dithiocarbamate Enhances Covalency. Nature. 2020 Jul;583(7816):396-9.

[177] Brown ID, Klages P, Skowron A. Influence of Pressure on the Lengths of Chemical Bonds. Acta Crystallogr. 2003;B59:439-48.

[178] Cammi R. Linear Chains of Hydrogen Molecules under Pressure: An Extreme-Pressure Continuum Model Study. J Chem Phys. 2019 Apr;150(16):164122.

[179] Casati N, Kleppe A, Jephcoat AP, Macchi P. Putting Pressure on Aromaticity along with in Situ Experimental Electron Density of a Molecular Crystal. Nat Commun. 2016;7:10901.

[180] Qiu L, Peña-Alvarez M, Baonza VG, Taravillo M, Casado J, Kertesz M. Mechanochemistry in [6]Cycloparaphenylene: A Combined Raman Spectroscopy and Density Functional Theory Study. ChemPhysChem. 2018 Aug;19(15):1903-16.

[181] Stauch T. Mechanical Switching of Aromaticity and Homoaromaticity in Molecular Optical Force Sensors for Polymers. Chem Eur J. 2018;24:7340-4.

[182] Fedorov AYu, Rychkov DA. COMPARISON OF DIFFERENT COMPUTATIONAL APPROACHES FOR UNVEILING THE HIGH-PRESSURE BEHAVIOR OF ORGANIC CRYSTALS AT A MOLECULAR LEVEL. CASE STUDY OF TOLAZAMIDE POLYMORPHS. J Struct Chem. 2020 Sep;61(9):1356-66.

[183] Montisci F, Lanza A, Casati N, Macchi P. $NO_2 \cdots NO_2$ Contacts under Compression: Testing the Forces in Soft Donor–Acceptor Interactions. Cryst Growth Des. 2018 Dec;18(12):7579-89.

[184] Montisci F, Ernst M, Macchi P. Experimental and Computational Study on the Effects of High Pressure on the Crystal Structure of Boron Nitrilotriacetate. Cryst Growth Des. 2023 Apr;23(4):2745-54.

[185] Hsieh CM, Grabbet B, Zeller F, Benter S, Scheele T, Sieroka N, et al. Can a Finite Chain of Hydrogen Cyanide Molecules Model a Crystal? ChemPhysChem. 2022;23:e202200414.

[186] Kumar KS, Ruben M. Sublimable Spin-Crossover Complexes: From Spin-State Switching to Molecular Devices. Angew Chem Int Ed. 2021;60:7502-21.

[187] Hogue RW, Singh S, Brooker S. Spin Crossover in Discrete Polynuclear Iron(II) Complexes. Chem Soc Rev. 2018;47:7303-38.

[188] Wolny JA, Paulsen H, Trautwein AX, Schünemann V. Density Functional Theory Calculations and Vibrational Spectroscopy on Iron Spin-Crossover Compounds. Coord Chem Rev. 2009 Oct;253(19-20):2423-31.

[189] Gaspar AB, Molnár G, Rotaru A, Shepherd HJ. Pressure Effect Investigations on Spin-Crossover Coordination Compounds. C R Chim. 2018 Dec;21(12):1095-120.

[190] Banerjee H, Chakraborty S, Saha-Dasgupta T. Design and Control of Cooperativity in Spin-Crossover in Metal–Organic Complexes: A Theoretical Overview. Inorganics. 2017 Jul;5(3):47.

[191] Wolny JA, Diller R, Schünemann V. Vibrational Spectroscopy of Mono- and Polynuclear Spin-Crossover Systems. Eur J Inorg Chem. 2012 Jun;2012(16):2635-48.

[192] Bousseksou A, Molnár G, Salmon L, Nicolazzi W. Molecular Spin Crossover Phenomenon: Recent Achievements and Prospects. Chem Soc Rev. 2011;40(6):3313.

[193] Gütlich P, Ksenofontov V, Gaspar AB. Pressure Effect Studies on Spin Crossover Systems. Coord Chem Rev. 2005;249:1811-29.

[194] Ksenofontov V, Gaspar AB, Gütlich P. Pressure Effect Studies on Spin Crossover and Valence Tautomeric Systems. Top Curr Chem. 2004;235:23-64.

[195] Wu Z, Wentzcovitch RM. Spin Crossover in Ferropericlase and Velocity Heterogeneities in the Lower Mantle. Proc Natl Acad Sci USA. 2014 Jul;111(29):10468-72.

[196] Javaid S, Javed Akhtar M. Pressure-Induced Magnetic, Structural, and Electronic Phase Transitions in $LaFeO_3$: A Density Functional Theory (Generalized Gradient Approximation) + U Study. J Appl Phys. 2014 Jul;116(2):023704.

[197] Wu Z, Justo JF, Wentzcovitch RM. Elastic Anomalies in a Spin-Crossover System: Ferropericlase at Lower Mantle Conditions. Phys Rev Lett. 2013 May;110(22):228501.

[198] Javaid S, Javed Akhtar M, Ahmad I, Younas M, Shah SH, Ahmad I. Pressure Driven Spin Crossover and Isostructural Phase Transition in $LaFeO_3$. J Appl Phys. 2013 Dec;114(24):243712.

[199] Goffinet M, Íñiguez J, Ghosez P. First-Principles Study of a Pressure-Induced Spin Transition in Multiferroic Bi 2 FeCrO 6. Phys Rev B. 2012 Jul;86(2):024415.

[200] Tarafder K, Kanungo S, Oppeneer PM, Saha-Dasgupta T. Pressure and Temperature Control of Spin-Switchable Metal-Organic Coordination Polymers from *Ab Initio* Calculations. Phys Rev Lett. 2012 Aug;109(7):077203.

[201] Hsu H, Yu YG, Wentzcovitch RM. Spin Crossover of Iron in Aluminous MgSiO3 Perovskite and Post-Perovskite. Earth Planet Sci Lett. 2012 Dec;359–360:34-9.

[202] Wojdeł JC, Moreira IDPR, Illas F. Periodic Density Functional Theory Study of Spin Crossover in the Cesium Iron Hexacyanochromate Prussian Blue Analog. J Chem Phys. 2009 Jan;130(1):014702.

[203] Wentzcovitch RM, Justo JF, Wu Z, da Silva CRS, Yuen DA, Kohlstedt D. Anomalous Compressibility of Ferropericlase throughout the Iron Spin Cross-Over. Proc Nat Acad Sci USA. 2009;106(21):8447-52.

[204] Bengtson A, Persson K, Morgan D. Ab Initio Study of the Composition Dependence of the Pressure-Induced Spin Crossover in Perovskite (Mg1-x,Fex)SiO3. Earth Planet Sci Lett. 2008 Jan;265(3-4):535-45.

[205] Bouldi N, Mannini M, Retegan M, Miller RG, Cahier B, Sainctavit P, et al. XAS and XMCD Reveal a Cobalt(II) Imide Undergoes High-Pressure-Induced Spin Crossover. J Phys Chem C. 2022;126:5784-92.

[206] Akiyoshi R, Komatsumaru Y, Donoshita M, Dekura S, Yoshida Y, Kitagawa H, et al. Ferroelectric Spin Crossover Cobalt(II) Compound Induced by Polar Ligand Substituent Motion. Angew Chem Int Ed. 2021;60:12717-22.

[207] Nguyen TAD, Veauthier JM, Angles-Tamayo GF, Chavez DE, Lapsheva E, Myers TW, et al. Correlating Mechanical Sensitivity with Spin Transition in the Explosive Spin Crossover Complex $[Fe(Htrz)_3]_n[ClO_4]_{2n}$. J Am Chem Soc. 2020 Mar;142(10):4842-51.

[208] Ioannidis EI, Kulik HJ. Towards Quantifying the Role of Exact Exchange in Predictions of Transition Metal Complex Properties. J Chem Phys. 2015;143:034104.

[209] Paulsen H, Schünemann V, Wolny JA. Progress in Electronic Structure Calculations on Spin-Crossover Complexes. Eur J Inorg Chem. 2013 Feb;2013(5-6):628-41.

[210] Cramer CJ, Truhlar DG. Density Functional Theory for Transition Metals and Transition Metal Chemistry. Phys Chem Chem Phys. 2009;11(46):10757.

[211] Daku LML, Vargas A, Hauser A, Fouqueau A, Casida ME. Assessment of Density Functionals for the High-Spin/Low-Spin Energy Difference in the Low-Spin Iron(II) Tris(2,2'-Bipyridine) Complex. ChemPhysChem. 2005;6:1393-410.

[212] Kajikawa S, Muraoka A. Theoretical Study of the Fe(Btr)2(NCS)2 Spin-Crossover Complex with Reparameterized Density Functionals. Chem Phys Lett. 2020 Jan;738:136867.

[213] Slimani A, Yu X, Muraoka A, Boukheddaden K, Yamashita K. Reparametrization Approach of DFT Functionals Based on the Equilibrium Temperature of Spin-Crossover Compounds. J Phys Chem A. 2014 Oct;118(39):9005-12.

[214] Reiher M. Theoretical Study of the Fe(Phen) $_2$ (NCS) $_2$ Spin-Crossover Complex with Reparametrized Density Functionals. Inorg Chem. 2002 Dec;41(25):6928-35.

[215] Matar S, Guionneau P, Chastanet G. Multiscale Experimental and Theoretical Investigations of Spin Crossover FeII Complexes: Examples of [Fe(Phen)2(NCS)2] and [Fe(PM-BiA)2(NCS)2]. Int J Mol Sci. 2015 Feb;16(2):4007-27.

[216] Jureschi CM, Rusu I, Codjovi E, Linares J, Garcia Y, Rotaru A. Thermo- and Piezochromic Properties of [Fe(Hyptrz)]A2·H2O Spin Crossover 1D Coordination Polymer: Towards Spin Crossover Based Temperature and Pressure Sensors. Physica B: Condens Matter. 2014 Sep;449:47-51.

[217] Bondì L, Brooker S, Totti F. Accurate Prediction of Pressure and Temperature T 1/2 Variation in Solid State Spin Crossover by Ab Initio Methods: The [CoII(Dpzca)2] Case. J Mater Chem C. 2021;9:14256-68.

[218] Chakraborty A, Chakraborty A, Ghosh S, Dasgupta I. Theoretical Analysis of Pressure Induced Spin Crossover Phenomenon in a Di-Nuclear Fe(II) Molecular Complex. J Phys Condens Matter. 2020 Apr;32(16):165802.

[219] Thiel AM, Damgaard-Møller E, Overgaard J. High-Pressure Crystallography as a Guide in the Design of Single-Molecule Magnets. Inorg Chem. 2020;59:1682-91.

[220] Ye HZ, Sun C, Jiang H. Monte-Carlo Simulations of Spin-Crossover Phenomena Based on a Vibronic Ising-like Model with Realistic Parameters. Phys Chem Chem Phys. 2015;17(10):6801-8.

[221] Butler IS, editor. High-Pressure Molecular Spectroscopy. Berlin/Boston: De Gruyter; 2022.

[222] Liu Y, Zeng Q, Zou B, Liu Y, Xu B, Tian W. Piezochromic Luminescence of Donor-Acceptor Cocrystals: Distinct Responses to Anisotropic Grinding and Isotropic Compression. Angew Chem Int Ed. 2018 Nov;57(48):15670-4.

[223] Banerjee H, Rittsteuer A, Aichhorn M. Temperature and Pressure Driven Spin Transitions and Piezochromism in a Mn-based Hybrid Perovskite. Phys Rev Mater. 2022 Apr;6(4):044401.

[224] Shi Y, Zhao W, Ma Z, Xiao G, Zou B. Self-Trapped Exciton Emission and Piezochromism in Conventional 3D Lead Bromide Perovskite Nanocrystals under High Pressure. Chem Sci. 2021;12(44):14711-7.

[225] Ma Y, Zhang L, Tang Y, Wu S, Tong ML, Wang K, et al. Pressure-Induced Piezochromism and Structure Transitions in Lead-Free Layered Cs $_4$ MnBi $_2$ Cl $_{12}$ Quadruple Perovskite. ACS Appl Energy Mater. 2021 Aug;4(8):7513-8.

[226] Wang L, Yao P, Wang F, Li S, Chen Y, Xia T, et al. Pressure-Induced Structural Evolution and Bandgap Optimization of Lead-Free Halide Double Perovskite (NH $_4$) $_2$ SeBr $_6$. Adv Sci. 2020 Mar;7(6):1902900.

[227] Jaffe A, Lin Y, Beavers CM, Voss J, Mao WL, Karunadasa HI. High-Pressure Single-Crystal Structures of 3D Lead-Halide Hybrid Perovskites and Pressure Effects on Their Electronic and Optical Properties. ACS Cent Sci. 2016 Apr;2(4):201-9.

[228] Beran GJO, Sugden IJ, Greenwell C, Bowskill DH, Pantelides CC, Adjiman CS. How Many More Polymorphs of ROY Remain Undiscovered. Chem Sci. 2022;13(5):1288-97.

[229] Feng X, Becke AD, Johnson ER. Computational Modeling of Piezochromism in Molecular Crystals. J Chem Phys. 2020 Jun;152(23):234106.

[230] Liu J, Du G, Liang N, Yang L, Feng Y, Chen Y, et al. Tunable Near-Infrared Piezochromic Luminescence by Effective Substituent Modification of D–A Structures. J Mater Chem C. 2023;11(25):8609-15.

[231] Aziz A, Sidat A, Talati P, Crespo-Otero R. Understanding the Solid State Luminescence and Piezochromic Properties in Polymorphs of an Anthracene Derivative. Phys Chem Chem Phys. 2022;24(5):2832-42.

[232] Irii S, Ogaki T, Miyashita H, Nobori K, Ozawa Y, Abe M, et al. Remarkable Piezofluorochromism of an Organoboron Complex Containing [2.2]Paracyclophane. Tetrahedron Lett. 2022;101:153913.

[233] Man Z, Lv Z, Xu Z, Liao Q, Liu J, Liu Y, et al. Highly Sensitive and Easily Recoverable Excitonic Piezochromic Fluorescent Materials for Haptic Sensors and Anti-Counterfeiting Applications. Adv Funct Mater. 2020 Apr;30(17):2000105.

[234] Zhang T, Shi W, Wang D, Zhuo S, Peng Q, Shuai Z. Pressure-Induced Emission Enhancement in Hexaphenylsilole: A Computational Study. J Mater Chem C. 2019;7(5):1388-98.

[235] Qi Q, Qian J, Tan X, Zhang J, Wang L, Xu B, et al. Remarkable Turn-On and Color-Tuned Piezochromic Luminescence: Mechanically Switching Intramolecular Charge Transfer in Molecular Crystals. Adv Funct Mater. 2015 Jul;25(26):4005-10.

[236] Sui Q, Ren XT, Dai YX, Wang K, Li WT, Gong T, et al. Piezochromism and Hydrochromism through Electron Transfer: New Stories for Viologen Materials. Chem Sci. 2017;8(4):2758-68.

[237] Lu S, Xiao G, Sui L, Feng T, Yong X, Zhu S, et al. Piezochromic Carbon Dots with Two-photon Fluorescence. Angew Chem Int Ed. 2017 May;56(22):6187-91.

[238] Wang X, Liu Q, Yan H, Liu Z, Yao M, Zhang Q, et al. Piezochromic Luminescence Behaviors of Two New Benzothiazole–Enamido Boron Difluoride Complexes: Intra- and Inter-Molecular Effects Induced by Hydrostatic Compression. Chem Commun. 2015;51(35):7497-500.

[239] Guo ZH, Jin ZX, Wang JY, Pei J. A Donor–Acceptor–Donor Conjugated Molecule: Twist Intramolecular Charge Transfer and Piezochromic Luminescent Properties. Chem Commun. 2014;50(46):6088.

[240] Chen F, Zhang J, Wan X. Design and Synthesis of Piezochromic Materials Based on Push-Pull Chromophores: A Mechanistic Perspective. Chem Eur J. 2012 Apr;18(15):4558-67.

[241] Zhao J, Zeng Y, Zheng X. Conformational Flexibility-Controlled Piezochromic Behavior of Organic Fluorophores. Chem Mater. 2022 Dec;34(23):10711-20.

[242] Zhai C, Yin X, Niu S, Yao M, Hu S, Dong J, et al. Molecular Insertion Regulates the Donor-Acceptor Interactions in Cocrystals for the Design of Piezochromic Luminescent Materials. Nat Commun. 2021 Jul;12(1):4084.

[243] Li G, Ren X, Shan G, Che W, Zhu D, Yan L, et al. New AIE-active Dinuclear Ir(III) Complexes with Reversible Piezochromic Phosphorescence Behaviour. Chem Commun. 2015;51(65):13036-9.

[244] Shan GG, Li HB, Zhu DX, Su ZM, Liao Y. Intramolecular π-Stacking in Cationic Iridium(Iii) Complexes with a Triazole–Pyridine Type Ancillary Ligand: Synthesis, Photophysics, Electrochemistry Properties and Piezochromic Behavior. J Mater Chem. 2012;22(25):12736.

[245] Byrne PJ, Richardson PJ, Chang J, Kusmartseva AF, Allan DR, Jones AC, et al. Piezochromism in Nickel Salicylaldoximato Complexes: Tuning Crystal-Field Splitting with High Pressure. Chem Eur J. 2012 Jun;18(25):7738-48.

[246] Lu Z, Archambault CM, Li S, Syed U, Wang S, Kumar A, et al. Modulating the Extent of Anisotropic Cuprophilicity via High Pressure with Piezochromic Luminescence Sensitization. J Phys Chem Lett. 2023 Jan;14(2):508-15.

[247] von Hopffgarten M, Frenking G. Energy Decomposition Analysis. WIREs Comput Mol Sci. 2012;2(1):43-62.

[248] Förster C, Osthues H, Schwab D, Doltsinis NL, Heinze K. Quantum Chemical Study of the Pressure-dependent Phosphorescence of [Cr(Ddpd)2]3+ in the Solid State. ChemPhysChem. 2023:DOI: e202300165.

[249] Azadi S, Foulkes WMC. Fate of Density Functional Theory in the Study of High-Pressure Solid Hydrogen. Phys Rev B. 2013;88:014115.

[250] Pickard CJ, Martinez-Canales M, Needs RJ. Density Functional Theory Study of Phase IV of Solid Hydrogen. Phys Rev B. 2012 Jun;85(21):214114.

[251] Azadi S, Monserrat B, Foulkes WMC, Needs RJ. Dissociation of High-Pressure Solid Molecular Hydrogen: A Quantum Monte Carlo and Anharmonic Vibrational Study. Phys Rev Lett. 2014 Apr;112(16):165501.

[252] Landerville AC, Oleynik II. Vibrational and Thermal Properties of β-HMX and TATB from Dispersion Corrected Density Functional Theory. AIP Conf Proc. 2017;1793:050007.

[253] Miao MS, Dreger ZA, Winey JM, Gupta YM. Density Functional Theory Calculations of Pressure Effects on the Vibrational Structure of α-RDX. J Phys Chem A. 2008 Nov;112(47):12228-34.

[254] Liu H, Zhao J, Wei D, Gong Z. Structural and Vibrational Properties of Solid Nitromethane under High Pressure by Density Functional Theory. J Chem Phys. 2006 Mar;124(12):124501.

[255] Zhu W, Zhang X, Wei T, Xiao H. DFT Studies of Pressure Effects on Structural and Vibrational Properties of Crystalline Octahydro-1,3,5,7-Tetranitro-1,3,5,7-Tetrazocine. Theor Chem Acc. 2009 Oct;124(3-4):179-86.

[256] Pagliai M, Cardini G, Cammi R. Vibrational Frequencies of Fullerenes C60 and C70 under Pressure Studied with a Quantum Chemical Model Including Spatial Confinement Effect. J Phys Chem A. 2014;118:5098-111.

[257] Kumar S, Weiß R, Zeller F, Neudecker T. Trapping the Transition State in a [2,3]-Sigmatropic Rearrangement by Applying Pressure. ACS Omega. 2022 Nov;7:45208-14.

[258] Boccalini M, Cammi R, Pagliai M, Cardini G, Schettino V. Toward an Understanding of the Pressure Effect on the Intramolecular Vibrational Frequencies of Sulfur Hexafluorid. J Phys Chem A. 2021;125:6362-73.

[259] Pagliai M, Cammi R, Cardini G, Schettino V. XP-PCM Calculations of High Pressure Structural and Vibrational Properties of P4S3. J Phys Chem A. 2016;120:5136-44.

[260] Fontana L, Santoro M, Bini R, Vinh DQ, Scandolo S. High-Pressure Vibrational Properties of Polyethylene. j Chem Phys. 2010 Nov;133(20):204502.

[261] Liu X, Michalchuk AAL, Bhattacharya B, Yasuda N, Emmerling F, Pulham CR. High-Pressure Reversitbility in a Plastically Flexible Coordination Polymer Crystal. Nat Commun. 2021;12:3871.

[262] Lenhardt JM, Ong MT, Choe R, Evenhuis CR, Martínez TJ, Craig SL. Trapping a Diradical Transition State by Mechanochemical Polymer Extension. Science. 2010;329:1057-60.

[263] Qiu ZY, Zhao X, Dang JS. Bowl-Shaped Carbon Skeletons under Tensile Stress: Quantum Mechanochemistry of Corannulene. New J Chem. 2023;47(13):6050-3.

[264] Diels O, Alder K. Synthesen in der hydroaromatischen Reihe. Justus Liebigs Ann Chem. 1928;460(1):98-122.

[265] Fringuelli F, Taticchi A. The Diels–Alder Reaction: Selected Practical Methods. 1st ed. John Wiley & Sons, Ltd; 2002.

[266] Nicolaou KC, Snyder SA, Montagnon T, Vassilikogiannakis G. The Diels–Alder Reaction in Total Synthesis. Angew Chem Int Ed. 2002;41(10):1668-98.

[267] Funel JA, Abele S. Industrial Applications of the Diels–Alder Reaction. Angew Chem Int Ed. 2013;52(14):3822-63.

[268] Wessig P, Müller G. The Dehydro-Diels-Alder Reaction. Chem Rev. 2008 Jun;108(6):2051-63.

[269] Klaerner FG, Krawczyk B, Ruster V, Deiters UK. Evidence for Pericyclic and Stepwise Processes in the Cyclodimerization of Chloroprene and 1,3-Butadiene from Pressure Dependence and Stereochemistry. Experimental and Theoretical Volumes of Activation and Reaction. J Am Chem Soc. 1994 Aug;116(17):7646-57.

[270] Chen B, Houk KN, Cammi R. High-Pressure Reaction Profiles and Activation Volumes of 1,3-Cyclohexadiene Dimerizations Computed by the Extreme Pressure-Polarizable Continuum Model (XP-PCM). Chem Eur J. 2022;28(29):e202200246.

[271] Stewart SG, Harfoot GJ, McRae KJ, Teng Y, Yu LJ, Chen B, et al. High-Pressure-Promoted and Facially Selective Diels–Alder Reactions of Enzymatically Derived Cis-1,2-Dihydrocatechols and Their Acetonide Derivatives: Enantiodivergent Routes to Homochiral and Polyfunctionalized Bicyclo[2.2.2]Octenes. J Org Chem. 2020 Oct;85(20):13080-95.

[272] Yang T, Fukuda R, Cammi R, Ehara M. Diels-Alder Cycloaddition of Cyclopentadiene and C60 at the Extreme High Pressure. J Phys Chem A. 2017;121:4363-71.

[273] Yoshimura Y, Osugi J, Nakahara M. Volumetric Study on the 1,3-Dipolar Cycloaddition Reaction. 2. Alpha-Benzoyl-N-phenylnitrone with Several Olefins. J Am Chem Soc. 1983 Aug;105(16):5414-8.

[274] Basilevsky MV, Weinberg NN, Zhulin VM. Pressure Dependence of Activation and Reaction Volumes. J Chem Soc, Faraday Trans 1. 1985;81(4):875.

[275] Basilevsky MV, Ryaboi VM, Weinberg NN. Nonequilibrium Effects in Kinetics of Cycloaddition Reactions under High Pressure. J Phys Chem. 1991 Jul;95(14):5533-40.

[276] Deglint E, Martens H, Edwards E, Boon N, Dance P, Weinberg N. Molecular Dynamics Calculation of Activation Volumes. Phys Chem Chem Phys. 2011;13(2):438-40.

[277] Loco D, Spezia R, Cartier F, Chataigner I, Piquemal JP. Solvation Effects Drive the Selectivity in Diels–Alder Reaction under Hyperbaric Conditions. Chem Commun. 2020;56(49):6632-5.

[278] Gao D, Tang X, Zhang C, Wang Y, Yang X, Zhang P, et al. Arylazo under Extreme Conditions: [2 + 2] Cycloaddition and Azo Metathesis. J Phys Chem C. 2023 Apr:acs.jpcc.3c01450.

[279] Zholdassov YS, Yuan L, Garcia SR, Kwok RW, Boscoboinik A, Valles DJ, et al. Acceleration of Diels-Alder Reactions by Mechanical Distortion. Science. 2023 Jun;380(6649):1053-8.

[280] Mathew N, Sewell T. Pressure-Dependent Elastic Coefficients of β-HMX from Molecular Simulations. Propellants Explos Pyrotech. 2018;43(3):223-7.

[281] Aslam TD, Bolme CA, Ramos KJ, Cawkwell MJ, Ticknor C, Price MA, et al. Shock to Detonation Transition of Pentaerythritol Tetranitrate (PETN) Initially Pressed to 1.65 g/Cm ^{3}. J Appl Phys. 2021 Jul;130(2):025901.

[282] Cai W, Zhang R, Yao Y, Deemyad S. Piezochromism and Structural and Electronic Properties of Benz[a]Anthracene under Pressure. Phys Chem Chem Phys. 2017;19(8):6216-23.

[283] Engelke R, Blais NC. Chemical Dimerization of Crystalline Anthracene Produced by Transient High Pressure. J Chem Phys. 1994 Dec;101(12):10961-72.

[284] Citroni M, Ceppatelli M, Bini R, Schettino V. Dimerization and Polymerization of Isoprene at High Pressures. J Phys Chem B. 2007 Apr;111(15):3910-7.

[285] Walling C, Peisach J. Organic Reactions Under High Pressure. IV. The Dimerization of Isoprene ^{1}. J Am Chem Soc. 1958 Nov;80(21):5819-24.

[286] Goncharov AF, Manaa MR, Zaug JM, Gee RH, Fried LE, Montgomery WB. Polymerization of Formic Acid under High Pressure. Phys Rev Lett. 2005 Feb;94(6):065505.

[287] Davydov VA, Kashevarova LS, Rakhmanina AV, Senyavin VM, Pronina OP, Oleynikov NN, et al. Pressure-Induced Dimerization of Fullerene C60: A Kinetic Study. Chem Phys Lett. 2001 Jan;333(3-4):224-9.

[288] Blank VD, Buga SG, Dubitsky GA, Serebryanaya NR, Popov MYu, Sundqvist B. HIGH-PRESSURE POLYMERIZED PHASES OF C60. Carbon. 1998;36(4):319-43.

[289] Citroni M, Ceppatelli M, Bini R, Schettino V. The High-Pressure Chemistry of Butadiene Crystal. J Chem Phys. 2003 Jan;118(4):1815-20.

[290] Citroni M, Ceppatelli M, Bini R, Schettino V. Laser-Induced Selectivity for Dimerization Versus Polymerization of Butadiene Under Pressure. Science. 2002;295:2058-60.

[291] Mugnai M, Cardini G, Schettino V. Charge Separation and Polymerization of Hydrocarbons at an Ultrahigh Pressure. Phys Rev B. 2004;70:020101.

[292] Stolte N, Yu J, Chen Z, Sverjensky DA, Pan D. Water-Gas Shift Reaction Produces Formate at Extreme Pressures and Temperatures in Deep Earth Fluids. J Phys Chem Lett. 2021;12:4292-8.

[293] Tassone F, Chiarotti GL, Rousseau R, Scandolo S, Tosatti E. Dimerization of CO2 at High Pressure and Temperature. ChemPhysChem. 2005;6:1752-6.

[294] Focher P, Chiarotti GL, Bernasconi M, Tosatti E, Parrinello M. Structural Phase Transformations via First-Principles Simulation. Europhys Lett. 1994 May;26(5):345-51.

[295] Serra S, Cavazzoni C, Chiarotti GL, Scandolo S, Tosatti E. Pressure-Induced Solid Carbonates from Molecular CO2 by Computer Simulation. Science. 1999 Apr;284(5415):788-90.

[296] Gohr S, Grimme S, Söhnel T, Paulus B, Schwerdtfeger P. Pressure Dependent Stability and Structure of Carbon Dioxide—A Density Functional Study Including Long-Range Corrections. J Chem Phys. 2013 Nov;139(17):174501.

[297] Yao Y, Klug DD, Martoňák R, Patchkovskii S. Dimerization of Boron Triiodide at High Pressure. Phys Rev B. 2011;83:214105.

[298] Yao Y, Hoffmann R. BH_3 under Pressure: Leaving the Molecular Diborane Motif. J Am Chem Soc. 2011 Dec;133(51):21002-9.

[299] Abe K, Ashcroft NW. Crystalline Diborane at High Pressures. Phys Rev B. 2011 Sep;84(10):104118.

[300] Liew KM, Ji WM, Zhang LW. Carbon Nanothreads Materials. Materials Horizons: From Nature to Nanomaterials. Singapore: Springer Singapore; 2022.

[301] Demingos PG, Balzaretti NM, Muniz AR. First-Principles Study of Carbon Nanothreads Derived from Five-Membered Heterocyclic Rings: Thiophene, Furan and Pyrrole. Physical Chemistry Chemical Physics. 2021;23(3):2055-62.

[302] Fu Y, Wu J, Xiao S, Liu S, Zhang Z, He J. Tensile Mechanical Characteristics of Ultra-Thin Carbon Sulfur Nanothreads in Orientational Order. Carbon. 2021 Oct;184:146-55.

[303] Fu Y, Xu K, Wu J, Zhang Z, He J. The Effects of Morphology and Temperature on the Tensile Characteristics of Carbon Nitride Nanothreads. Nanoscale. 2020;12(23):12462-75.

[304] Marutheeswaran S, Jemmis ED. Adamantane-Derived Carbon Nanothreads: High Structural Stability and Mechanical Strength. J Phys Chem C. 2018 Apr;122(14):7945-50.

[305] Zhan H, Zhang G, Tan VBC, Gu Y. The Best Features of Diamond Nanothread for Nanofibre Applications. Nat Commun. 2017 Apr;8(1):14863.

[306] Silveira JFRV, Muniz AR. First-Principles Calculation of the Mechanical Properties of Diamond Nanothreads. Carbon. 2017 Mar;113:260-5.

[307] Feng C, Xu J, Zhang Z, Wu J. Morphology- and Dehydrogenation-Controlled Mechanical Properties in Diamond Nanothreads. Carbon. 2017 Nov;124:9-22.

[308] Roman RE, Kwan K, Cranford SW. Mechanical Properties and Defect Sensitivity of Diamond Nanothreads. Nano Lett. 2015 Mar;15(3):1585-90.

[309] Chen B, Crespi VH, Hoffmann R. Theoretical Studies of Furan and Thiophene Nanothreads: Structures, Cycloaddition Barriers, and Activation Volumes. J Am Chem Soc. 2022 May;144(20):9044-56.

[310] Lloyd EM, Vakil JR, Yao Y, Sottos NR, Craig SL. Covalent Mechanochemistry and Contemporary Polymer Network Chemistry: A Marriage in the Making. J Am Chem Soc. 2023 Jan:DOI: jacs.2c09623.

[311] Ghanem MA, Basu A, Behrou R, Boechler N, Boydston AJ, Craig SL, et al. The Role of Polymer Mechanochemistry in Responsive Materials and Additive Manufacturing. Nat Rev Mater. 2020:DOI: 10.1038/s41578-02000249w.

[312] Küng R, Göstl R, Schmidt BM. Release of Molecular Cargo from Polymer Systems by Mechanochemistry. Chem Eur J. 2022;28:e202103860.

[313] Shen H, Cao Y, Lv M, Sheng Q, Zhang Z. Polymer Mechanochemistry for Release of Small Cargoes. Chem Commun. 2022;58:4813-24.

[314] Versaw BA, Zeng T, Hu X, Robb MJ. Harnessing the Power of Force: Development of Mechanophores for Molecular Release. J Am Chem Soc. 2021;143(51):21461-73.

[315] Mier LJ, Adam G, Kumar S, Stauch T. The Mechanism of Flex-Activation in Mechanophores Revealed By Quantum Chemistry. ChemPhysChem. 2020;21:2402-6.

[316] Larsen MB, Boydston AJ. "Flex-activated" Mechanophores: Using Polymer Mechanochemistry To Direct Bond Bending Activation. J Am Chem Soc. 2013;135:8189-92.

[317] Traeger H, Kiebala DJ, Weder C, Schrettl S. From Molecules to Polymers - Harnessing Inter- and Intramolecular Interactions to Create Mechanochromic Materials. Macromol Rapid Commun. 2021;42:2000573.

[318] He S, Stratigaki M, Centeno SP, Dreuw A, Göstl R. Tailoring the Properties of Optical Force Probes for Polymer Mechanochemistry. Chem Eur J. 2021;64:15889-97.

[319] Davis DA, Hamilton A, Yang J, Cremar LD, van Gough D, Potisek SL, et al. Force-Induced Activation of Covalent Bonds in Mechanoresponsive Polymeric Materials. Nature. 2009;459:68-72.

[320] Li W. Mechanophores in Polymer Mechanochemistry: Insights from Single-Molecule Experiments and Computer Simulations. In: Zhou Y, Chou HH, editors. Functional Tactile Sensors. Duxford: Elsevier; 2021. p. 113-40.

[321] Jung S, Yoon HJ. Heterocyclic Mechanophores in Polymer Mechanochemistry. Synlett. 2022;33:863-74.

[322] Binder WH. The "labile" Chemical Bond: A Perspective on Mechanochemistry in Polymers. Polymer. 2020;202:122639.

[323] Klein IM, Husic CC, Kovács DP, Choquette NJ, Robb MJ. Validation of the CoGEF Method as a Predictive Tool for Polymer Mechanochemistry. J Am Chem Soc. 2020;142:16364-81.

[324] De Bo G. Polymer Mechanochemistry and the Emergence of the Mechanophore Concept. Macromolecules. 2020;53:7615-7.

[325] Kumar S, Zeller F, Stauch T. A Two-Step Baromechanical Cycle for Repeated Activation and Deactivation of Mechanophores. J Phys Chem Lett. 2021;12:9470-4.

[326] Li M, Zhang Q, Zhou YN, Zhu S. Let Spiropyran Help Polymers Feel Force! Prog Polym Sci. 2018;79:26-39.

[327] Liu Y, Su X, Li N, Wang K, Li Q, Shao W, et al. Real Time Optical Monitoring of Cascade Mechanochemical Reaction and Capture of Ultra-Unstable Intermediate under Hydrostatic Pressure. Mater Chem Front. 2023:10.1039.D3QM00282A.

[328] Kabb CP, O'Bryan CS, Morley CD, Angelini TE, Sumerlin BS. Anthracene-Based Mechanophores for Compression-Activated Fluorescence in Polymeric Networks. Chem Sci. 2019;10:7702-8.

[329] Koo B, Nofen E, Chattopadhyay A, Dai L. Dimeric Anthracene-Based Mechanophore for Damage Precursor Detection in Epoxy-Based Thermoset Polymer Matrix: Characterization and Atomistic Modeling. Comput Mater Sci. 2017;133:167-74.

[330] Meng X, Qi G, Li X, Wang Z, Wang K, Zou B, et al. Spiropyran-Based Multi-Colored Switching Tuned by Pressure and Mechanical Grinding. J Mater Chem C. 2016;4:7584-8.

[331] Meng X, Qi G, Zhang C, Wang K, Zou B, Ma Y. Visible Mechanochromic Responses of Spiropyrans in Crystals via Pressure-Induced Isomerization. Chem Commun. 2015;51:9320-3.

[332] Fukuda R, Nakatani K. Quantum Chemical Study on the High-Pressure Effect for [4 + 4] Retrocycloaddition of Anthracene Cyclophane Photodimer [Research-Article]. J Phys Chem C. 2019;123(7):4493-501.

[333] Miao MS. Caesium in High Oxidation States and as a P-Block Element. Nat Chem. 2013;5:846-52.

[334] Wessel C, Dronskowski R. A First-Principles Study on Chromium Sesquioxide, Cr2O3. J Solid State Chem. 2013 Mar;199:149-53.

[335] Selli D, Baburin IA, Martoňák R, Leoni S. Novel Metastable Metallic and Semiconducting Germaniums. Sci Rep. 2013;3:1466.

[336] Wang H, Tse JS, Tanaka K, Iitaka T, Ma Y. Superconductive Sodalite-like Clathrate Calcium Hydride at High Pressures. Proc Nat Acad Sci USA. 2012;109(17):6463-6.

[337] Lin J, Du X, Rahm M, Yu H, Xu H, Yang G. Exploring the Limits of Transition-Metal Fluorination at High Pressures. Angew Chem Int Ed. 2020;59(23):9155-62.

[338] Yao Y, Tse JS, Klug DD. Structures of Insulating Phases of Dense Lithium. Phys Rev Lett. 2009;102:115503.

[339] Vítek A, Arismendi-Arrieta DJ, Rodríguez-Cantano R, Prosmiti R, Villarreal P, Kalus R, et al. Computational Investigations of the Thermodynamic Properties of Size-Selected Water and Ar–Water Clusters: High-Pressure Transitions. Phys Chem Chem Phys. 2015;17(14):8792-801.

[340] Hermann A, Ashcroft NW, Hoffmann R. High Pressure Ices. Proc Natl Acad Sci USA. 2012 Jan;109(3):745-50.

[341] Santra B, Klimeš J, Alfè D, Tkatchenko A, Slater B, Michaelides A, et al. Hydrogen Bonds and van Der Waals Forces in Ice at Ambient and High Pressures. Phys Rev Lett. 2011 Oct;107(18):185701.

[342] Santra B, Klimeš J, Tkatchenko A, Alfè D, Slater B, Michaelides A, et al. On the Accuracy of van Der Waals Inclusive Density-Functional Theory Exchange-Correlation Functionals for Ice at Ambient and High Pressures. J Chem Phys. 2013 Oct;139(15):154702.

[343] Murray ÉD, Galli G. Dispersion Interactions and Vibrational Effects in Ice as a Function of Pressure: A First Principles Study. Phys Rev Lett. 2012 Mar;108(10):105502.

[344] Kang D, Dai J, Yuan J. Changes of Structure and Dipole Moment of Water with Temperature and Pressure: A First Principles Study. J Chem Phys. 2011;135:024505.

[345] Imoto S, Marx D. How Can Protons Migrate in Extremely Compressed Liquid Water? Phys Rev Lett. 2020;125:086001.

[346] Rustad JR, Yuen DA, Spera FJ. Molecular Dynamics of Liquid SiO2 under High Pressure. Phys Rev A. 1990;42(4):2081-9.

[347] Horbach J. Molecular Dynamics Computer Simulation of Amorphous Silica under High Pressure. J Phys: Condens Matter. 2008;20:244118.

[348] Zeidler A, Wezka K, Rowlands RF, Whittaker DAJ, Salmon PS, Polidori A, et al. High-Pressure Transformation of SiO2 Glass from a Tetrahedral to an Octahedral Network: A Joint Approach Using Neutron Diffraction and Molecular Dynamics. Phys Rev Lett. 2014;113:135501.

[349] Zhang S, Morales MA, Jeanloz R, Millot M, Hu SX, Zurek E. Nature of the Bonded-to-Atomic Transition in Liquid Silica to TPa Pressures. J Appl Phys. 2022 Feb;131(7):071101.

[350] Dulmage WJ, Lipscomb WN. The Crystal Structures of Hydrogen Cyanide, HCN. Acta Cryst. 1951 Jul;4(4):330-4.

[351] MacKenzie GA, Pawley GS. A Neutron Scattering Study of DCN. J Chem Phys C: Solid State Phys. 1979;12:2715-35.

[352] Chall M, Winkler B, Milman V. Ab Initio Calculation of the High-Pressure Behaviour of Hydrogen Cyanide. J Phys: Condens Matter. 1996;8:9049-57.

[353] Khazaei M, Liang Y, Bahramy MS, Pichierri F, Esfarjani K, Kawazoe Y. High-Pressure Phases of Hydrogen Cyanide: Formation of Hydrogenated Carbon Nitride Polymers and Layers and Their Electronic Properties. J Phys: Condens Matter. 2011;23:405403.

[354] Peng J, Zhang S, Refson K, Dove MT. The Ferroelastic Phase Transition in Hydrogen Cyanide Studied by Density Functional Theory. J Phys: Condens Matter. 2022 Mar;34(9):095402.

[355] Caratelli C, Cammi R, Chelli R, Pagliai M, Cardini G, Schettino V. Insights on the Realgar Crystal under Pressure from XP-PCM and Periodic Model Calculations. J Phys Chem A. 2017;121(46):8825-34.

[356] Melicherová D, Martoňák R. Study of Polymerization of High-Pressure Nitrogen by Ab Initio Molecular Dynamics. J Chem Phys. 2023 Jun;158(24):244503.

[357] Boates B, Bonev SA. First-Order Liquid-Liquid Phase Transition in Compressed Nitrogen. Phys Rev Lett. 2009 Jan;102(1):015701.

[358] Attaccalite C, Sorella S. Stable Liquid Hydrogen at High Pressure by a Novel Ab Initio Molecular-Dynamics Calculation. Phys Rev Lett. 2008;100:114501.

[359] Labet V, Gonzalez-Morelos P, Hoffmann R, Ashcroft NW. A Fresh Look at Dense Hydrogen under Pressure. I. An Introduction to the Problem, and an Index Probing Equalization of H–H Distances. J Chem Phys. 2012 Feb;136(7):074501.

[360] Labet V, Hoffmann R, Ashcroft NW. A Fresh Look at Dense Hydrogen under Pressure. II. Chemical and Physical Models Aiding Our Understanding of Evolving H–H Separations. J Chem Phys. 2012 Feb;136(7):074502.

[361] Labet V, Hoffmann R, Ashcroft NW. A Fresh Look at Dense Hydrogen under Pressure. III. Two Competing Effects and the Resulting Intra-Molecular H-H Separation in Solid Hydrogen under Pressure. J Chem Phys. 2012 Feb;136(7):074503.

[362] Labet V, Hoffmann R, Ashcroft NW. A Fresh Look at Dense Hydrogen under Pressure. IV. Two Structural Models on the Road from Paired to Monatomic Hydrogen, via a Possible Non-Crystalline Phase. J Chem Phys. 2012 Feb;136(7):074504.

[363] Naumov II, Hemley RJ, Hoffmann R, Ashcroft NW. Chemical Bonding in Hydrogen and Lithium under Pressure. J Chem Phys. 2015 Aug;143(6):064702.

[364] Bardeen J, Cooper LN, Schrieffer JR. Theory of Superconductivity. Phys Rev. 1957 Dec;108(5):1175-204.

[365] Ashcroft NW. Metallic Hydrogen: A High-Temperature Superconductor? Phys Rev Lett. 1968 Dec;21(26):1748-9.

[366] Feng J, Grochala W, Jaroń T, Hoffmann R, Bergara A, Ashcroft NW. Structures and Potential Superconductivity in SiH 4 at High Pressure: En Route to "Metallic Hydrogen". Phys Rev Lett. 2006 Jan;96(1):017006.

[367] Kurzydłowski D, Grochala W. Phonon Dispersion Analysis as an Indispensable Tool for Predictions of Solid State Polymorphism and Dynamic Metastability: Case of Compressed Silane D. Acta Phys Pol A. 2011;119(6):895-900.

[368] Flores-Livas JA, Amsler M, Lenosky TJ, Lehtovaara L, Botti S, Marques MAL, et al. High-Pressure Structures of Disilane and Their Superconducting Properties. Phys Rev Lett. 2012;108:117004.

[369] Baettig P, Zurek E. Pressure-Stabilized Sodium Polyhydrides: NaH n (n > 1). Phys Rev Lett. 2011 Jun;106(23):237002.

[370] Labet V, Hoffmann R, Ashcroft NW. Molecular Models for WH6 under Pressure. New Journal of Chemistry. 2011;35(10):2349.

[371] Gao G, Hoffmann R, Ashcroft NW, Liu H, Bergara A, Ma Y. Theoretical Study of the Ground-State Structures and Properties of Niobium Hydrides under Pressure. Phys Rev B. 2013 Nov;88(18):184104.

[372] Huan TD, Amsler M, Marques MAL, Botti S, Willand A, Goedecker S. Low-Energy Polymeric Phases of Alanates. Phys Rev Lett. 2013;110:135502.

[373] Hooper J, Terpstra T, Shamp A, Zurek E. Composition and Constitution of Compressed Strontium Polyhydrides. J Phys Chem C. 2014 Mar;118(12):6433-47.

[374] Shamp A, Zurek E. Superconducting High-Pressure Phases Composed of Hydrogen and Iodine. J Phys Chem Lett. 2015 Oct;6(20):4067-72.

[375] Ye X, Hoffmann R, Ashcroft NW. Theoretical Study of Phase Separation of Scandium Hydrides under High Pressure. J Phys Chem C. 2015 Mar;119(10):5614-25.

[376] Bi T, Miller DP, Shamp A, Zurek E. Superconducting Phases of Phosphorus Hydride Under Pressure: Stabilization by Mobile Molecular Hydrogen. Angew Chem Int Ed. 2017;56(34):10192-5.

[377] Zarifi N, Bi T, Liu H, Zurek E. Crystal Structures and Properties of Iron Hydrides at High Pressure. The Journal of Physical Chemistry C. 2018 Oct;122(42):24262-9.

[378] Ye X, Zarifi N, Zurek E, Hoffmann R, Ashcroft NW. High Hydrides of Scandium under Pressure: Potential Superconductors. J Phys Chem C. 2018 Mar;122(11):6298-309.

[379] Bi T, Zurek E. Electronic Structure and Superconductivity of Compressed Metal Tetrahydrides. Chem Eur J. 2021;27(60):14858-70.

[380] Jaroń T, Ying J, Tkacz M, Grzelak A, Prakapenka VB, Struzhkin VV, et al. Synthesis, Structure, and Electric Conductivity of Higher Hydrides of Ytterbium at High Pressure. Inorg Chem. 2022 Jun;61(23):8694-702.

[381] Zurek E, Bi T. High-Temperature Superconductivity in Alkaline and Rare Earth Polyhydrides at High Pressure: A Theoretical Perspective. J Chem Phys. 2019 Feb;150(5):050901.

[382] Wen XD, Hoffmann R, Ashcroft NW. Benzene under High Pressure: A Story of Molecular Crystals Transforming to Saturated Networks, with a Possible Intermediate Metallic Phase. J Am Chem Soc. 2011 Jun;133(23):9023-35.

[383] Li X, Baldini M, Wang T, Chen B, Xu Es, Vermilyea B, et al. Mechanochemical Synthesis of Carbon Nanothread Single Crystals. J Am Chem Soc. 2017 Nov;139(45):16343-9.

[384] Amsler M, Flores-Livas JA, Lehtovaara L, Balima F, Ghasemi SA, MacHon D, et al. Crystal Structure of Cold Compressed Graphite. Phys Rev Lett. 2012;108:065501.

[385] Wen XD, Hand L, Labet V, Yang T, Hoffmann R, Ashcroft NW, et al. Graphane Sheets and Crystals under Pressure. Proc Natl Acad Sci USA. 2011 Apr;108(17):6833-7.

[386] González-Cataldo F, Godwal BK, Driver K, Jeanloz R, Militzer B. Model of Ramp Compression of Diamond from Ab Initio Simulations. Phys Rev B. 2021 Oct;104(13):134104.

[387] Wang X, Proserpio DM, Oses C, Toher C, Curtarolo S, Zurek E. The Microscopic Diamond Anvil Cell: Stabilization of Superhard, Superconducting Carbon Allotropes at Ambient Pressure. Angew Chem Int Ed. 2022;134(32):e202205129.

[388] Martin W, Baross J, Kelley D, Russell MJ. Hydrothermal Vents and the Origin of Life. Nat Rev Microbiol. 2008 Nov;6(11):805-14.

[389] Morowitz HJ, Srinivasan V, Smith E. Ligand Field Theory and the Origin of Life as an Emergent Feature of the Periodic Table of Elements. Biol Bull. 2010 Aug;219(1):1-6.

[390] Kitchen DB, Reed LH, Levy RM. Molecular Dynamics Simulation of Solvated Protein at High Pressure. Biochemistry. 1992;31:10083-93.

[391] Roche J, Louis JM, Bax A, Best RB. Pressure-Induced Structural Transition of Mature HIV-1 Protease from a Combined NMR/MD Simulation Approach. Proteins: Struct, Funct, Bioinformatics. 2015;83:2117-23.

[392] Song G, Lancelon-Pin C, Chen P, Yu J, Zhang J, Su L, et al. Time-Dependent Elastic Tensor of Cellulose Nanocrystal Probed by Hydrostatic Pressure and Uniaxial Stretching. J Phys Chem Lett. 2021;12:3779-85.

[393] Goldman N, Reed EJ, Fried LE, Kuo IFW, Maiti A. Synthesis of Glycine-Containing Complexes in Impacts of Comets on Early Earth. Nat Chem. 2010;2:949-54.

[394] Yan H, Yang F, Pan D, Lin Y, Hohman JN, Solis-Ibarra D, et al. Sterically Controlled Mechanochemistry under Hydrostatic Pressure. Nature. 2018;554:505-10.